ИЗВЕСТИЯ ВЫСШИХ УЧЕБНЫХ ЗАВЕДЕНИЙ.
Т 62 (11) Серия «**ХИМИЯ И ХИМИЧЕСКАЯ ТЕХНОЛОГИЯ**» 2019

IZVESTIYA VYSSHIKH UCHEBNYKH ZAVEDENII
V 62 (11) **KHIMIYA KHIMICHESKAYA TEKHNOLOGIYA** 2019
RUSSIAN JOURNAL OF CHEMISTRY AND CHEMICAL TECHNOLOGY

DOI: 10.6060/ivkkt.20196211.5913.3

УДК:

СПЕКТРОСКОПИЧЕСКИ И / ИЛИ СТРУКТУРНО ИНТРИГУЮЩИЕ ФТАЛОЦИАНИНЫ И ПОДОБНЫЕ СОЕДИНЕНИЯ. ЧАСТЬ 3. ДИМЕРНЫЕ СИСТЕМЫ, ТЕТРАМЕРЫ И ВЫВОДЫ

Н. Кобаяши

Нагао Кобаяши

Кафедра химии и материалов, факультет текстильной науки и технологии, университет Шиншу, Уеда, 386-8567, Япония
E-mail: nagaok@shinshu-u.ac.jp, nagao.kobayashi.c3@tohoku.ac.jp

Данная работа является третьей частью обзора, в котором представлены свойства большой группы фталоцианинов, которые были синтезированы и спектроскопически и теоретически изучены в работах, выполненных под руководством автора за период 2007-2017 гг. Приведены примеры анализа спектроскопических данных в сочетании с квантово-химическими расчетами различного уровня. В качестве спектроскопических методов использовались методы электронного поглощения, естественного и магнитного кругового дихроизма (CD и MCD) флуоресценции, фосфоресценции и электронного парамагнитного резонанса с временным разрешением. На основе квантово-химических расчетов теоретически проанализированы спектры (4n + 2) π систем, а также некоторые 4nπ антиароматических систем. В отличие от первой и второй частей обзора, в данной части рассматриваются димерные и тетрамерные системы.

Ключевые слова: фталоцианины, энергия, МО, строение, спектры

SPECTROSCOPICALLY AND/OR STRUCTURALLY INTRIGUING PHTHALOCYANINES AND RELATED COMPOUNDS. PART 3. DIMERIC SYSTEMS, TETRAMERS, AND CONCLUSIONS

N. Kobayashi

Nagao Kobayashi

Department of Chemistry and Materials, Faculty of Textile Science and Technology, Shinshu University, Ueda 386-8567, Japan
E-mail: nagaok@shinshu-u.ac.jp, nagao.kobayashi.c3@tohoku.ac.jp

This work is the third part of the review, which presents the properties of a large group of phthalocyanines, which were synthesized and spectroscopically and theoretically studied in works performed under the guidance of the author for the period 2007-2017. Examples of the analysis of spectroscopic data in combination with quantum-chemical calculations of different level are given. As spectroscopic methods, we used the methods of electron absorption, natural and magnetic circular dichroism (CD and MCD) fluorescence, phosphorescence, and electron paramagnetic resonance with time resolution. Based on quantum-chemical calculations, the spectra of (4n + 2) π systems, as well as some 4nπ antiaromatic systems, were theoretically analyzed. Unlike the first and second parts of the review, this part deals with dimeric and tetrameric systems.

Key words: phthalocyanines, energy, MO, structure, spectra

Для цитирования:
Кобаяши Н. Спектроскопически и / или структурно интригующие фталоцианины и подобные соединения. Часть 3. Димерные системы, тетрамеры и выводы. *Изв. вузов. Химия и хим. технология*. 2019. Т. 62. Вып. 11. С. 4–37
For citation:
Kobayashi N. Spectroscopically and/or structurally intriguing phthalocyanines and related compounds. Part 3. Dimeric systems, tetramers, and conclusions. *Izv. Vyssh. Uchebn. Zaved. Khim. Khim. Tekhnol*. 2019. V. 62. N 11. P. 4–37

DIMERIC SYSTEMS

Cofacial Types

a) A μ-oxo Hetero Dimer of Silicon Phthalocyanine and Naphthalocyanine [1]

The structures and properties of μ-oxo SiPc dimers have been intensively investigated as the smallest component of μ-oxo cofacial dimers from the early stage of this chemistry. Staggered orientation of Pc monomer units with a torsion angle (θ) of 36.6° was reported for the crystal structure of the peripherally unsubstituted SiPc dimer [2], whereas free rotation of the Pc units was inferred in solution from the NMR analysis. μ-Oxo SiPc dimers generally exhibit blue-shifted Q band absorption at ca. 630 nm as compared to that of the corresponding SiPc monomers [2, 3] which is intuitively interpreted in terms of the exciton coupling interaction between the cofacially arranged monomer units. However, it is now assumed that the absorption spectral feature of μ-oxo SiPc dimers is better illustrated by taking interchromophore interactions into consideration. Recently, we have succeeded in synthesizing a novel μ-oxo hetero dimer comprising SiPc and silicon naphthalocyanine (SiNc). To our surprise, in chloroform this hetero dimer exhibited only a single intense band in the Q band region of the SiPc monomer and no intense band in the Q band region of the SiNc monomer. This absorption spectrum does not appear to be a simple summation of the absorption spectra of SiPc and SiNc. Here, in-depth insight into the unique Q band absorption and solvatochromic behavior is provided based on the X-ray crystal structure analysis, variable temperature NMR measurements, and theoretical calculations on possible rotational isomers.

μ-Oxo SiPc–SiNc dimer **5** was obtained from conventional thermal condensation reaction of peripherally butoxy-substituted SiPc **1** and SiNc **2** in quinoline at 180 °C in 20-25% yield along with μ-oxo homo dimers **3** and **4** (Scheme 1). Since severe aggregation of **5** prevented its characterization by ^{1}H NMR, axial ligand exchange reaction from hydroxy groups to bulky triphenylsilyloxy groups was conducted to give **6** almost quantitatively.

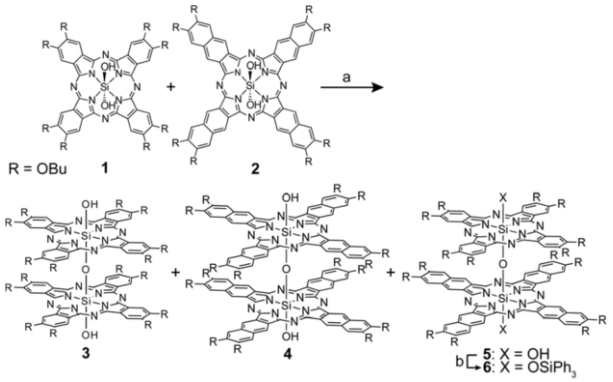

Scheme 1. Synthesis of μ-oxo dimers. Reaction conditions: (a) quinoline, 180°C, 3 h; (b) quinoline, 180°C, 1 d
Схема 1. Синтез μ -оксодимеров. Условия реакции: (а) хинолин, 180 ° С, 3 ч; (b) хинолин, 180 ° С, 1 д

The ^{1}H NMR spectrum of **6** in $CDCl_3$ at room temperature exhibited a singlet peak at 8.26 ppm due to the benzo moieties of the SiPc unit and two singlet peaks at 9.22 and 7.97 ppm due to the naphthalene moieties of the SiNc unit, while the phenyl protons of the axial triphenylsilyloxy groups were observed at 6.27 (*para*), 6.20 (*para*), 5.77 (*meta*), 5.65 (*meta*), 3.99 (*ortho*), and 3.85 (*ortho*) ppm due to the different ring current effects of the SiPc and SiNc units. This signal pattern allowed us to infer a C_{4v} (θ = 0° or 45°) symmetric conformation for **6** or fast rotation of the Pc and Nc planes in chloroform at room temperature. Finally the structure of **6** was unambiguously elucidated by X-ray diffraction analysis on crystals obtained from diffusion of methanol into a toluene solution of **6** (Fig. 1). In the crystal structure, the axial triphenylsilyloxy group of the SiPc unit was replaced by a methoxy group, during the growth of crystals in the presence of methanol. The interplanar distance between the SiPc and SiNc units is 3.3 Å, which is similar to those of μ-oxo homo dimers and polymers, whereas the torsion angle of θ = 18° is smaller than that of the unsubstituted μ-oxo SiPc dimer (θ = 36.6°) [2]. The different torsion angle of **6** in the solid state from that expected from the ^{1}H NMR spectrum in chloroform can be ascribed to the different solvent used for the crystallization or a packing force.

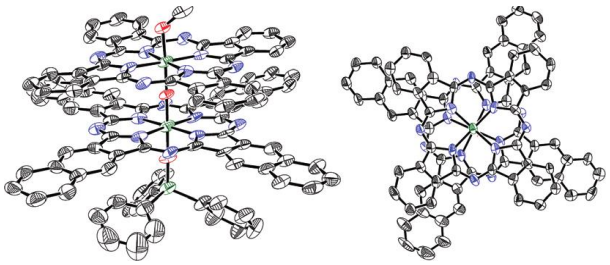

Fig. 1. Crystal structure of **6**. The thermal ellipsoids are scaled to the 50% probability level. In both views, hydrogen atoms and peripheral butoxy substituents and in the top view axial ligands are omitted for clarity

Рис. 1. Кристаллическая структура **6**. Тепловые эллипсоиды масштабируются до уровня вероятности 50%. На обоих изображениях атомы водорода и периферические бутокси-заместители и на виде сверху осевые лиганды опущены для ясности

The absorption spectrum of **6** in chloroform exhibits an intense Q band at 682 nm with a shoulder in both the longer and shorter wavelength regions, and the tail of the lower-energy absorption extends to 1200 nm (Fig. 2). The position of the main Q band is similar to that of the corresponding SiPc monomer (682 nm), and no intense absorption appears in the Q band region of the SiNc monomer (790 nm). This absorption spectrum is quite unique considering that the absorption spectra of all the other hetero dimers and oligomers are expressed as approximately simple summations of each component. Further investigation on the absorption spectra in several solvents revealed solvatochromic behavior of **6**. In toluene the absorption spectrum becomes broad without changing the positions of the main Q band absorption at 687 nm (Fig. 2). In addition, the shoulder absorption at around 600 nm and the broad absorption in the 800-900 nm region intensifies, whereas the weak absorption in the 1000-1200 nm region decreases further. This solvatochromic behavior is opposite to that observed for the peripherally alkoxy-substituted μ-oxo SiPc homo dimers, which exhibit broad absorption in non-aromatic solvents and intense Q band absorption in aromatic solvents [4, 5].

The MCD spectrum of **6** in chloroform shows a dispersion-type Faraday A term corresponding to the intense Q band at 682 nm, whereas several distinctive MCD signals are also observed with respect to the broad and featureless absorption in the region from 800 to 1200 nm (Fig. 2). The MCD spectrum of **6** in toluene exhibits a basically similar spectral shape, whereas decrease of the MCD signals in the region from 1000 to 1200 nm and intensification of the MCD signals corresponding to the longer and shorter shoulder absorption of the Q band are observed (Fig. 2). These basically similar MCD spectra over the entire region infer similar band components, but the intensity of the bands vary probably due to difference in interchromophore interactions of rotational isomers with different torsion angles.

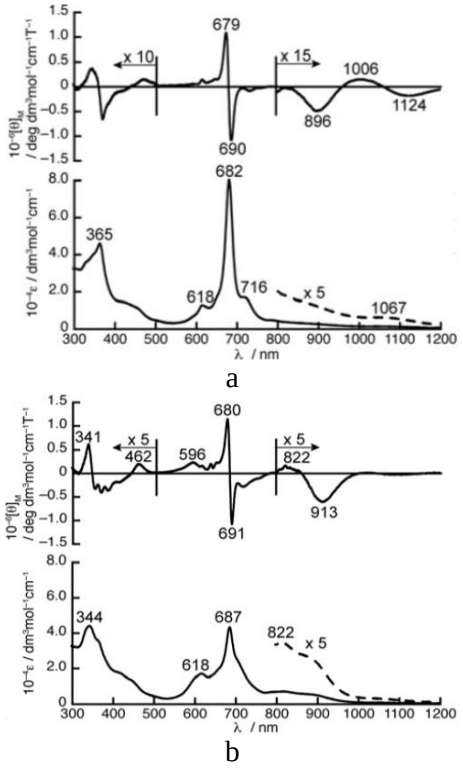

Fig. 2. Absorption (bottom) and MCD (top) spectra of **6** in (a) $CHCl_3$ and (b) toluene at room temperature

Рис. 2. Спектры поглощения (внизу) и МКД (вверху) **6** в (a) $CHCl_3$ и (b) толуоле при комнатной температуре

In order to obtain insight into the conformations in solution, variable temperature ^{1}H NMR measurements were performed in both $CDCl_3$ and toluene-d_8 (not shown). The ^{1}H NMR spectrum in $CDCl_3$ at -50 °C exhibited only a slight broadening of the non-peripheral proton signals, without significantly changing the chemical shifts. The observed signal patterns over the entire measured temperature ranges are indicative of a C_{4v} symmetric conformation with torsion angles of θ = 0° or 45° or a fast rotation within the NMR time scale. The ^{1}H NMR spectrum of **6** in toluene-d_8 at room temperature exhibited three sharp singlet peaks at 9.69, 8.58, and 7.85 ppm due to the non-peripheral protons. Upon lowering the temperature, these sharp signals were retained until -40 °C, while further decrease of the measurement temperature led to broadening of all the proton signals without any changes in the chemical shift. This result indicates the presence of thermally equilibrated rotational isomers in toluene.

The presence of thermally equilibrated rotational isomers was further confirmed by thermochromic behavior in toluene. Upon lowering the temperature to -80 °C, the Q band became intensified at

the expense of its shoulder absorption. The final absorption spectrum at -80 °C was approximately similar to that in chloroform, but the Q band at 688 nm was slightly red-shifted as compared to that at 682 nm in chloroform at room temperature.

DFT and TDDFT calculations at the B3LYP/6-31G(d) level were performed on model compounds of rotational isomers with torsion angles of $\theta = 0°$, 23°, and 45°. The TDDFT calculations reveal that the main absorption in the Q band region is composed of transitions from the HOMO and HOMO-1 to the degenerate LUMOs (LUMO and LUMO+1) and the secondly degenerate unoccupied orbitals (LUMO+2 and LUMO+3) for all the rotational isomers. The HOMO and HOMO-1 are localized on the Nc and Pc moieties, respectively, due to the higher HOMO energy level of the SiNc than that of the SiPc, whereas the four unoccupied orbitals (LUMO~LUMO+3) originate from linear combinations of the degenerate LUMOs (LUMO and LUMO+1) of the SiPc and SiNc monomers. These orbitals are, therefore, delocalized on both the Pc and Nc moieties. Based on the TDDFT calculations, theoretical absorption spectra of the rotational isomers with $\theta = 0°$ and 45° are approximately similar, exhibiting intense bands mainly comprising transitions from the HOMO-1 to the LUMOs (LUMO~LUMO+3) at 662 (oscillator strength (f) = 0.312) and 596 (f = 0.248) nm for $\theta = 0°$ and at 662 (f = 0.399) and 589 (f = 0.183) nm for $\theta = 45°$, followed by weak bands (transitions from the HOMO to the LUMO and LUMO+1) at 1009 nm (f = 0.0058, $\theta = 0°$) and 1050 nm (f = 0.0090, $\theta = 45°$) and moderate bands (transitions from the HOMO to the LUMO+2 and LUMO+3) at 787nm (f = 0.082, $\theta = 0°$) and 784 nm (f = 0.059, $\theta = 45°$).The smaller oscillator strengths of the transitions from the HOMO as compared to those from the HOMO-1 can be qualitatively ascribed to contribution of configuration interactions between these excited states. These spectral patterns appear to be in good agreement with the observed absorption spectra in chloroform and in toluene at low temperature. Despite similar band components in the theoretical absorption spectrum of the rotational isomer with $\theta = 23°$, the intensities and wavelengths vary so that the lowest energy bands are blue-shifted and the theoretical absorption becomes broad.

Based on both the experimental and theoretical results, it can be clearly concluded that a plausible conformation in chloroform is a C_{4v} symmetric rotational isomer with $\theta = 0°$ or 45°, whereas rotational isomers, a C_{4v} symmetric rotational isomer and less symmetric isomers with $0° < \theta < 45°$ are likely to be in equilibrium in toluene at room temperature, and a C_{4v} symmetric rotational isomer would become a predominant isomer upon lowering the temperature.

In summary, a novel μ-oxo hetero dimer of SiPc and SiNc was synthesized. In the solid state, this hetero dimer takes a C_4 symmetric conformation with a torsion angle of 18°, whereas the conformations in solution depend upon the solvent conditions, which is manifested by unique solvatochromic behavior. Based on the absorption and ^{1}H NMR spectra as well as theoretical calculations, **6** appears to adopt a conformation close to C_{4v} ($\theta = 0°$ or 45°) in chloroform, exhibiting an intense Q band with a shoulder in the lower energy region, whereas rotational isomers are in equilibrium at room temperature in toluene, causing broadening of the Q band absorption. Despite the difference in the molecular size, the interchromophore interactions between the SiPc and SiNc units become significant due to similar energies and symmetries of the degenerate LUMOs. These results suggest a possibility that spectroscopic properties of co-facial oligomers and the conduction band nature of co-facial polymers can be further controlled by assembling hetero monomer units with similar energies and symmetries of frontier molecular orbitals.

b) Definitive Assignments of the Visible–Near-IR Bands of Porphyrin-Naphthalocyanine Rare-Earth Sandwich Double- and Triple-Decker Compounds by Magnetic Circular Dichroism Spectroscopy [6]

Here, the MCD spectra of porphyrin-naphthalocyanine (Nc) rare-earth sandwich double- and triple-decker compounds are recorded in the range of 300-2000 nm, to gain a better understanding of the characteristic spectral features. The results are successfully explained on the basis of a simple molecular orbital (MO) model by considering the relevant interactions of Gouterman's four orbitals of the constituent chromophores [7]. The interpretation of the electronic absorption spectra of even homoleptic rare-earth sandwich complexes of phthalocyanines (Pcs) has not necessarily been consistent among researchers in the past. However, as will be elucidated, by comparing the spectra of a series of heteroleptic naphthalocyaninato and porphyrinato sandwich complexes, the assignments of the visible to near-IR absorption bands of these sandwich complexes become unambiguous.

Scheme 2 shows the structures of the sandwich complexes of the present study. The neutral form of the dimer is a radical complex in which the hole or unpaired electron is delocalized over the two rings. This has been confirmed by EPR, NMR, and IR spectroscopy. Since the interplanar distance of this type of complexes (2.65-3.06 Å) was closer than their van der

Waals distance (3.4 Å), electron exchange interactions play an important role in the electronic structures. In such a case, an MO model is more appropriate than an exciton model to understand the spectroscopic properties. Indeed, Ishikawa et al. successfully interpreted the spectral features of some homoleptic sandwich phthalocyanine complexes by calculating the MOs [8].

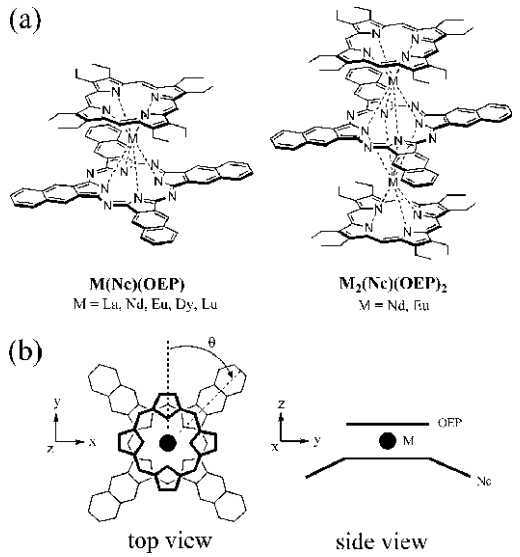

Scheme 2. (a) Compounds in this study. (b) Schematic geometry of the π skeletons of sandwich heterodimer (staggered conformation with twist angle θ = 45°) OEP = octaethylporphinato, Nc = naphthalocyaninato

Схема 2. (а) Соединения в этом исследовании. (b) Схематическая геометрия π-скелетов сэндвич-гетеродимера (ступенчатая конформация с углом закручивания θ = 45 °) OEP = октаэтилпорфинато, Nc = нафталоцианинато

The previous single-crystal X-ray analyses have revealed that the complexes (M(Nc)(OEP), M = La, Pr, Nd, Sm, Eu, Gd, Tb, Dy, Ho, Er, Yb, Lu, Y) adopt a conformation in which the two chromophoric units are almost fully staggered with respect to the pyrrole nitrogen atoms, regardless of the size of the central metal (Scheme 2b). Thus, the twist angle θ, defined as the rotation angle of one ring away from the eclipsed conformation of the two rings, is close to 45° (approximately C_{4v} symmetry) in the crystal structure. This is in contrast to the crystal structure of a series of bis(phthalocyaninato) lanthanide(III) complexes, in which the twist angle increases with decreasing size of the central metal. A series of the OEP-Nc dimers, therefore, appears to be an ideal system for analyzing their systematic spectral changes on the basis of MO models: conformational flexibilities, which sometimes cause unreliable MO analyses, are negligible in this system.

i) Neutral Form of M(Nc)(OEP)

Spectroscopic Properties. Typical electronic absorption and MCD spectra of the neutral form of sandwich dimers (La(Nc)(OEP) and Dy(Nc)(OEP)) in $CHCl_3$ are shown in Fig. 3, with the values of the spectra tabulated in Table 1, together with assignments of the bands to electronic transitions.

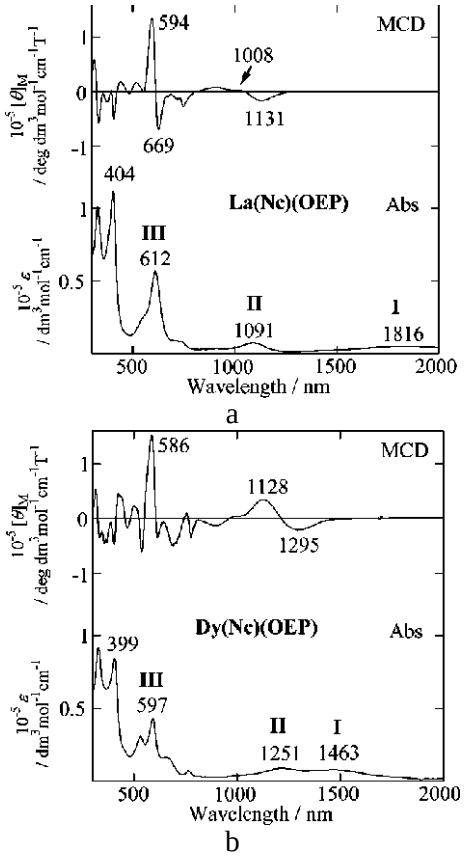

Fig. 3. Electronic absorption and MCD spectra of La(Nc)(OEP) (a) and Dy(Nc)(OEP) (b) recorded in $CHCl_3$ at room temperature

Рис. 3. Электронные спектры поглощения и МКД спектры La (Nc) (OEP) (a) и Dy (Nc) (OEP) (b), записанные в $CHCl_3$ при комнатной температуре

As we previously reported, the peak positions of the absorption bands depend strongly on the ionic radius of the central metal. Bands **I** and **II** undergo red- and blue-shifts, respectively, as the ionic radius increases, while the spectral shift of Band **III** is relatively small. It was found that the MCD signal corresponding to Band **I** is an extremely weak absorption-type signal, which can be attributed to a Faraday B term. In contrast, the MCD signals of Band **II** were assigned to a Faraday A term. The signal pattern of the Dy dimer has a typical first derivative shape, while that of the La dimer is less resolved. This may arise from overlap with a vibronic side band. The most intense MCD signals, which appear to be a first derivative of the absorption band, were observed at about 600 nm (Band **III**). This type of intense signal should be correlated to the Q-band nature with a large magnetic dipole moment. The intense absorption bands with weaker MCD signals seen at ca. 400 nm are attributable to the Soret bands.

Table 1

Electronic Absorption and MCD Data for the Neutral Form of [M(Nc)(OEP)] in the Near-IR Region in $CHCl_3$ at Room temperature

***Таблица 1*. Данные электронного поглощения и МКД для нейтральной формы [M (Nc) (OEP)] в ближней ИК области в $CHCl_3$ при комнатной температуре**

central metal (ionic radius)	assignment	abs λ (nm)	$10^{-4}\epsilon$ (dm^3 mol^{-1} cm^{-1})	MCD λ (nm)	$10^{-3}[\theta]_M$ (deg dm^3 mol^{-1} cm^{-1} T^{-1})
La	I	1816	0.29	1823	- 0.6
(116 pm)	II	1091	0.42	1131, 1008	- 16.4, 3.0
Nd	I	1642	0.58	1658	- 1.5
(110.9 pm)	II	1157	0.65	1196, 1060	- 28.4, 5.0
Eu	I	1542	0.58	1591	- 1.1
(106.6 pm)	II	1196	0.71	1244, 1102	- 22.0, 3.5
Dy	I	1463	0.72	1463(sh)	- 2.0
(102.7 pm)	II	1251	0.79	1295, 1128	- 20.5, 34.9
Lu	I (and II)	1336	0.78	1323, 1038	- 10.2, 4.1
(97.7 pm)					

Fig. 4 shows the dependence of the near-IR spectra on the size of the central rare-earth metal. It is clearly seen that the excitation energies corresponding to Bands **I** and **II** are systematically shifted and that the MCD appearances (sign and intensity) are essentially similar throughout the series. Assuming a systematic change, Bands **I** and **II** of the Lu complex are in the same absorption envelope. The absorption shoulder seen in the higher energy region of Band **II** may be a vibronic band of Band **II**.

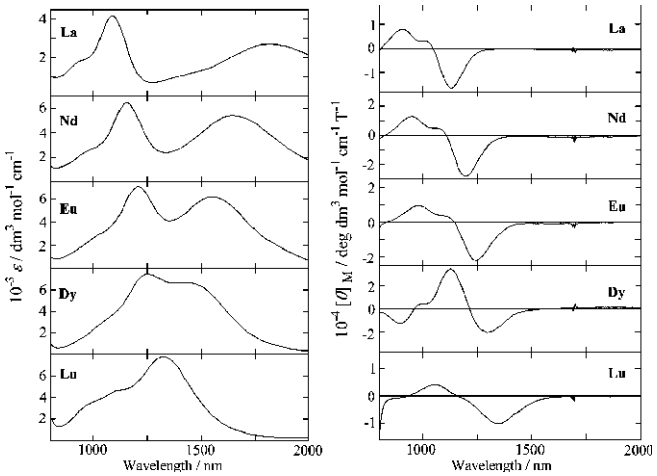

Fig. 4. Dependence of the central atom of the sandwich dimer (M(Nc)(OEP)) on the near-IR absorption (left) and MCD (right) spectra. The MCD signals at ca.1650 and 1800 nm are due to C-H vibration of the solvent ($CHCl_3$)

Рис. 4. Зависимость центрального атома сэндвич-димера (M (Nc) (OEP)) от спектров поглощения в ближней ИК-области (слева) и МКД (справа). Сигналы МКД при длине волны около 1650 и 1800 нм обусловлены колебаниями С-Н растворителя ($CHCl_3$)

MO Analysis. To explain the observed spectral features of the sandwich dimers, let us first introduce the relationship between the spectroscopic properties of monomeric OEP and Nc, and Gouterman's four orbitals. A metallo OEP generally exhibits a significantly weak visible absorption band at 500-600 nm (Q-band), while a metallo Nc shows sharp, intense Q-bands beyond 750 nm because of the extended π system.

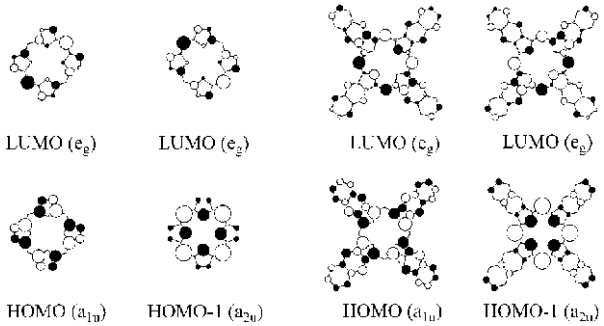

Fig. 5. Gouterman's four orbitals of OEP and Nc chromophores. Peripheral ethyl groups are omitted for clarity

Рис. 5. Четыре орбитали Гутермана с OEP и Nc хромофорами. Периферические этильные группы опущены для ясности

Fig. 5 shows Gouterman's four orbitals of OEP and Nc units. Both compounds have degenerate LUMO (e_g) because of D_{4h} symmetry. The coefficients of the degenerate LUMO can be arbitrarily chosen. As shown in Fig. 5, coefficients of the LUMOs are chosen to be matching canonical components of the degenerate symmetry representation when the sandwich dimer is formed. It is seen from Fig. 6 that the energy level of the HOMO-1 (a_{2u}) of OEP is close to that of the HOMO (a_{1u}).

As a result, a significant mixing of the HOMO and HOMO-1 to LUMO (degenerate) occurs, leading to cancellation of the transition moments in the Q-bands. In contrast, the a_{2u} orbital (HOMO-1) of the Nc is strongly stabilized because of the higher electronegativity of the *meso*-nitrogen atoms, while the a_{1u} orbital (HOMO) is considerably destabilized because of antibonding interactions with the fused naphthalene rings. This causes a smaller HOMO-LUMO gap and less mixing of these transitions, resulting in an intense near-IR Q transition.

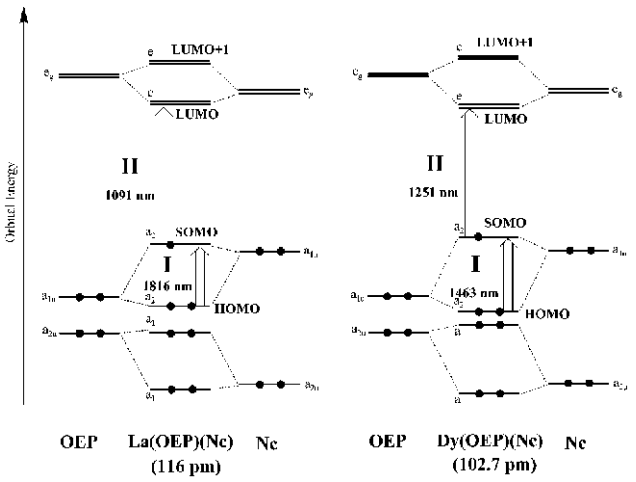

Fig. 6. Schematic representation of the frontier MO energies for the C_{4v} sandwich dimer (M(OEP)(Nc)) with larger (M = La) and smaller (M = Dy) central metals. The value in parentheses indicates the size of the central metal

Рис. 6. Схематическое представление граничных энергий МО для сэндвич-димера C_{4v} (M (OEP) (Nc)) с более крупными (M = La) и меньшими (M = Dy) центральными металлами. Значение в скобках указывает размер центрального металла

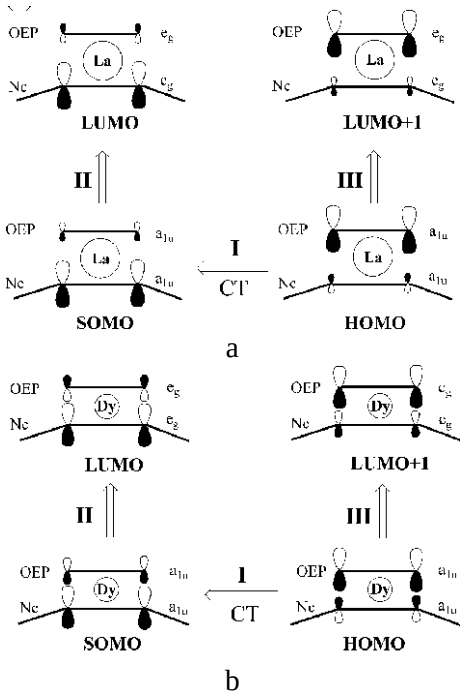

Fig. 7. Schematic representation of the bonding and antibonding interactions of (a) dimer with larger metal (b) dimer with smaller metal. The size of the orbital corresponds to the coefficient of the dimer's MOs

Рис. 7. Схематическое представление связывающих и антисвязывающих взаимодействий (a) димера с более крупным металлом (b) димера с более мелким металлом. Размер орбитали соответствует коэффициенту МО димера

An MO model comprising Gouterman's orbitals of OEP and Nc chromophores is then considered. In general, interaction with two monomeric MOs gives two new MOs, one of lower energy than the lower of the two monomeric MOs, the other of higher energy than the higher of the same two MOs. The MOs of the present dimer contain a greater contribution from the monomeric MO which is closer in energy to the new MO. Since the HOMO-LUMO gap of Nc is smaller than that of OEP, the following features can be deduced for the frontier MOs of the OEP-Nc system: the SOMO (singly occupied molecular orbital) and LUMO (degenerate) contain a greater contribution from Nc, while the HOMO and LUMO+1 (degenerate) have a greater contribution from OEP. Consequently, the schematic MO diagrams of a dimer with a large or small central metal become as illustrated in Fig. 6. Schematic illustrations of the bonding and antibonding interactions between the AOs are shown in Fig. 7.

First, it should be noted that there is no interaction between the a_{1u} and a_{2u} orbitals because of their different symmetry. In addition, we can assume that the pyrrole α carbon interactions (C_α-C_α) contribute mainly to the MOs of the dimer, since these moieties are the closest positions in the eclipsed conformation. This interaction is quite evident in the a_{1u}-a_{1u} interaction.

On the basis of the MO models, the absorption bands **I** and **II** can be assigned to the HOMO→SOMO and SOMO→LUMO transitions, respectively. These assignments are in agreement with the observed MCD signals: the HOMO(a_2)→SOMO(a_2) transition is a nondegenerate transition that has a CT character (from OEP to Nc), which correlates with the Faraday B term (absorption-shape MCD signal) observed in the MCD spectra. The transition polarization is parallel to the *z*-axis (see Scheme 2b). Since the transition moment between two states of a_2 symmetry has a_1 symmetry ($a_2 \times a_2 = a_1$), the transition becomes electric dipole allowed, but magnetic dipole forbidden on the basis of the group theory. The small intensity of the MCD may be essentially the result of the transfer character of the transition, which gives rise to small oscillator strength of the absorption spectrum. On the other hand, the SOMO(a_2)→LUMO(e) transition is a degenerate transition that has a π-π^* transition character (Nc's Q-band character) with *x*- or *y*-axis polarization, correlating with the Faraday A term observed in the MCD spectra. Since the π-π^* transition of porphynoids has a relatively large magnetic moment [7], an intense MCD signal is predicted. In addition, the MCD spectral shape observed for Band **II** is explained as follows. Since the SOMO→LUMO transition corresponds to the promotion of one electron from the antibonding a_2 orbital to the bonding e orbital, the potential energy curve of this state, along with the inter-macrocyclic distance coordinate, is expected to be displaced to give a shorter Nc-OEP distance, relative to the ground state. This

leads to a shift of the Franck-Condon intensity from the origin to higher vibronic components [9]. As a result, a significant convolution of the Franck-Condon 0-0 band and the vibronic bands occurs for Band **II**. The dome-shaped structure of the Nc ring may also contribute to the intensity redistribution. The weak absorption bands observed between Bands **II** and **III** (ca. 550-700 nm) may be ascribed to CT transitions such as the HOMO→LUMO (transition from OEP to Nc) and SOMO→LUMO+1 transitions (transition from Nc to OEP), judging from their optically forbidden nature.

The dependence of the size of the central metal on the absorption peak positions can be reasonably explained using the simple MO model. In the case of a larger central metal, the HOMO-SOMO energy gap is smaller than the SOMO-LUMO energy gap because of the smaller overlap between AOs corresponding to the pyrrole α-carbons. This causes the well-separated excitation energies of Bands **I** and **II**. In contrast, in the case of a smaller central metal, the HOMO-SOMO energy gap becomes comparable to the SOMO-LUMO energy gap because of the larger overlap between the monomeric MOs, so that the energy gap between Bands **I** and **II** decreases considerably. This MO model is consistent with the electrochemical properties, which showed a linear correlation between the redox potentials and the size of the central metal [10]. Here, the first oxidation potential, which is related to the SOMO energy, decreases when the ionic radius of the central metal becomes smaller.

As mentioned earlier, relatively intense MCD signals were observed for Band **III**. This should be related to the Q-band character, because the orbital angular momentum for the Q transition is in general larger than the other transitions [7]. Thus, Band **III** can be attributed to a transition having the OEP's Q-band character (HOMO→LUMO+1).

We now comment on the MCD signs observed for Band **II**. According to Michl's perimeter model, the sign sequence of Faraday A terms is predicted by assessing the orbital degeneracy of the frontier MOs [11-14]. When the LUMO and HOMO are degenerate and nondegenerate, a negative/positive first-derivative signal pattern is predicted with increasing energy. The MCD signals of high-symmetry porphyrin and related compounds have been in agreement with theory. The negative/positive MCD signs for Band **II** of the present dimers indicate that the degeneracy of the LUMO remains unchanged.

ii) Oxidized and Reduced Forms of M(Nc)(OEP). The neutral form of the dimer is reported to be easily oxidized or reduced by chemical or electrochemical methods [10]. The spectroscopic properties of the dimer vary dramatically, depending on the changes in molecular charge. For example, the spectra of the neutral, oxidized, and reduced forms of Eu(Nc)(OEP) are shown in Fig. 8. Two near-IR absorption bands observed at 1196 nm (band **II**) and 1542 nm (band **I**) for the neutral form disappeared in both the reduced and oxidized forms. A new absorption band appeared at 900 nm for the reduced form, while a new absorption band appeared at 1100 nm for the oxidized form. The MCD spectra clearly indicate a first-derivative pattern (Faraday A term) for the absorption band at 900 nm of $[Eu(Nc)(OEP)]^-$, while the absorption shape (Faraday B term) for the absorption at 1100 nm of $[Eu(Nc)(OEP)]^+$, thus indicating transitions to degenerate and nondegenerate states, respectively. The absorption and MCD spectral patterns of the other metal complexes are essentially identical to the Eu complexes, although the peak positions of the reduced and oxidized forms are also systematically changed, depending on the size of the central metal.

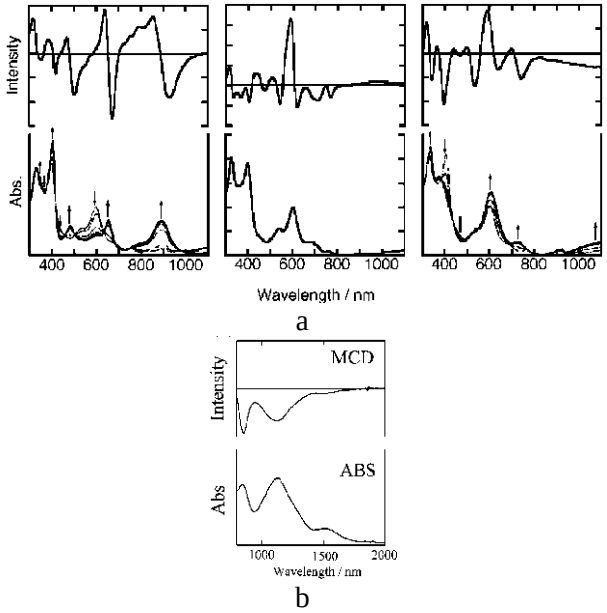

Fig. 8. (a) Electronic absorption and MCD spectra of the reduced, neutral, and oxidized form of Eu(Nc)(OEP) from left to right. (b) Electronic absorption and MCD spectra of $[Eu(Nc)(OEP)]^+$ in the near-IR region. The absorption at ca. 1500 nm may arise from the neutral form

Рис. 8. (a) Электронные спектры поглощения и МКД спектры восстановленной, нейтральной и окисленной формы Eu (Nc) (OEP) слева направо. (b) Электронные спектры поглощения и MCD спектры [Eu (Nc) (OEP)] + в ближней ИК-области. Поглощение при 1500 нм может принадлежать нейтральной форме

The simple MO model discussed in the previous section can account for the spectral changes of the reduced and oxidized systems. The oxidation process corresponds to the removal of one electron from the SOMO of the neutral form, while the reduction process corresponds to addition of one electron to the SOMO. The change in the number of electrons on the antibonding MO results in a geometrical change in the dimer:

in the case of the reduced dimer, the antibonding orbital (i.e., the SOMO of the neutral species) is filled with two electrons to become the HOMO, so that the Nc-OEP distance increases to some extent because of electrostatic repulsion between the two rings. This results in a smaller energy gap between the bonding (for example, HOMO-1) and antibonding (for example, HOMO) MOs, and as a result, the HOMO (Nc π)→LUMO (Nc π*) transition (corresponding to the SOMO→LUMO transition of the neutral form) shifts to the blue. In contrast, an electron on the antibonding occupied orbital (i.e., SOMO of the neutral species) is removed in the case of the oxidized form, leading to a smaller Nc-OEP distance because of the absence of the repulsion. This results in the observation of a blue-shift of the HOMO (OEP π)→LUMO (Nc π) transition (corresponding to the HOMO→SOMO transition of the neutral form). The changes in the simple MO levels are summarized in Fig. 9.

DFT Calculations. To confirm the validity of our simple MO models, geometry optimizations of the neutral, reduced, and oxidized dimers ([M(Nc)(OEP)], $[M(Nc)(OEP)]^-$, $[M(Nc)\text{-}(OEP)]^+$, M = La, Y) were carried out at the DFT/B3LYP level of theory. The peripheral ethyl groups were omitted and replaced with hydrogen, and the C_{4V} symmetry restriction was used.

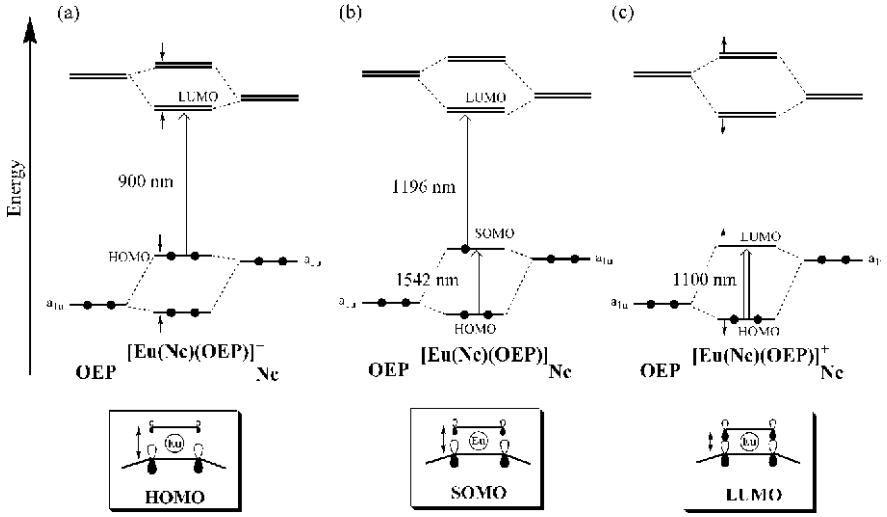

Fig. 9. Schematic representation of the relative MO energy of M(Nc)(OEP). (a) The reduced form, (b) the neutral form, and (c) the oxidized form
Рис. 9. Схематическое представление относительной энергии MO M (Nc) (OEP). (a) восстановленная форма, (b) нейтральная форма и (c) окисленная форма

As shown in Fig. 10, the converged structure of Y(Nc)(OEP) appears to be similar to the crystal structure previously reported [10]: (1) the metal center lies closer to the N_4 plane of OEP because of the larger cavity of the OEP ring: the cavity sizes, defined as the distance between the trans pyrrole nitrogen atoms, are 4.189 Å (OEP) and 4.032 Å (Nc). (2) The Nc ring is significantly domed.

The calculated geometrical parameters are in fairly good agreement with those of the crystal structure. This indicates that the peripheral ethyl substituent does not significantly affect the geometry of the sandwich complexes. The direction of the ethyl groups observed in the crystal structure may arise from the effect of crystal packing. Table 2 shows the distance between the nearest pyrrole α carbon atoms of the OEP and Nc rings ($D_{\alpha\alpha}$). This parameter would be directly related to the interaction between AOs on the pyrrole α carbon (C_α -C_α). According to Table 2, the value of $D_{\alpha\alpha}$ decreases in the order of reduced, neutral, and oxidized forms, so that the validity of the proposed MO model is verified.

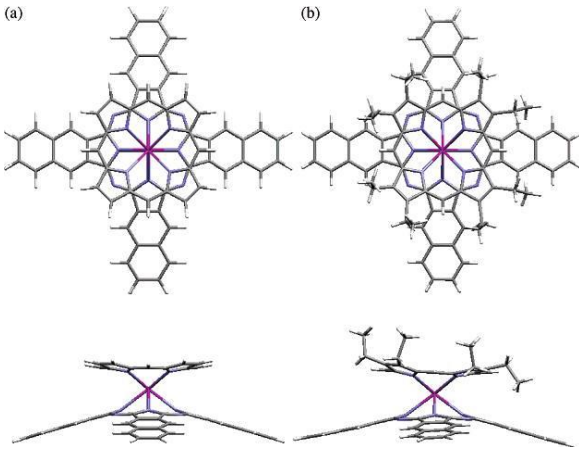

Fig. 10. Top and side view of the molecular structure of Y(Nc)(OEP). (a) Optimized structure (B3LYP/def-SV(P)). (b) Crystal structure
Рис. 10. Вид сверху и сбоку на молекулярную структуру Y (Nc) (OEP). (a) Оптимизированная структура (B3LYP / def-SV (P)). (b) кристаллическая структура

Table 2

Calculated Distance (Å) between the Nearest Pyrrole α Carbon Atoms (Dαα) for the Neutral, Oxidized, and Reduced Forms of the Sandwich Dimers (M(Nc)(OEP))

***Таблица 2.* Рассчитанное расстояние (Å) между ближайшими пиррольными α атомами углерода (Dαα) для нейтральных, окисленных и восстановленных форм димеров сэндвича (M (Nc) (OEP))**

central metal (ionic radius)	oxidized form	neutral form[a]	reduced form
La (116 pm)	3.634	3.677 (3.490)	3.699
Y (101.9 pm)	3.249	3.294 (3.167)	3.343

[a] The value in parentheses indicates the corresponding distance calculated from the crystal structure (ref [10])

[a] Значение в скобках указывает на соответствующее отклонение, вычисленное по кристаллической структуре (см. [10])

The calculated MO energy levels are given in Fig. 11. The calculated MO energy diagrams are essentially identical to those anticipated conceptionally: (1) the MOs of the sandwich dimer consist of linear combinations of the constituent monomeric MOs. (2) As the central metal becomes smaller, the bonding and antibonding energy splitting increases. Although the calculation shows that the energy of the bonding $25a_2$ orbital is lower than that of antibonding $44a_1$ orbital, the lowest optically allowed transition would still be the one between the a_2 orbitals, irrespective of the order of these two orbitals as indicated in Fig. 6. This comes from the fact that the $a_1 \rightarrow a_2$ jump is symmetry forbidden ($a_1 \times a_2 = a_2$). In addition, the effect of the peripheral ethyl groups may cause the destabilization of a_{1u} orbital of a monomeric porphyrin skeleton with D_{4h} symmetry.

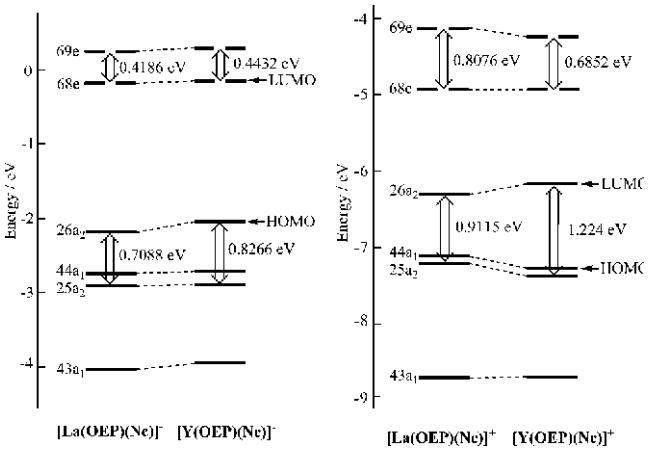

Fig. 11. Selected energy level scheme for the reduced forms (left) and oxidized forms (right) of La(Nc)(OEP) and Y(Nc)(OEP) obtained from DFT/ B3LYP/def-SV(P)

Рис. 11. Выбранная схема энергетического уровня для восстановленных форм (слева) и окисленных форм (справа) La (Nc) (OEP) и Y (Nc) (OEP), полученных из DFT / B3LYP / def-SV (P)

Neutral Form of the Sandwich Trimers, $M_2(Nc)(OEP)_2$

The above simple MO model for heteroleptic dimers can be applied to heteroleptic triple-decker systems that we have recently succeeded in preparing [10]. To date, only one crystal structure ($Nd_2(Nc)(OEP)_2$) is available. [10] According to the crystal structure, each OEP ring is not in an ideal staggered conformation with a twist angle of ca. 45°, but adopts a conformation with a twist angle of ca. 30°. However, in this work, we assume that the geometry of the triple-decker is a fully staggered conformation with D_{4h} symmetry in solution. The electronic absorption and MCD spectra of the triple-deckers ($M_2(Nc)(OEP)_2$, M = Nd, Eu) are given in Fig. 12. The lowest three absorption bands are labeled as Bands **I**, **II**, and **III**. All the MCD signals corresponding to Bands **I**, **II**, and **III** can be attributed to Faraday A terms because of their first derivative type shapes. As the metal size decreases, the absorption peak of Band **I** shifts considerably to longer wavelength, while that of Bands **II** and **III** almost do not vary. There is no absorption band attributable to a CT band from one chromophore to the other chromophore, unlike Band **I** of the sandwich dimers.

Fig. 13 indicates a schematic MO energy diagram for the triple-decker system. Note that the neutral form of the trimer is not a radical complex, in contrast to the heteroleptic dimeric M(Nc)(OEP) system. The HOMO of the trimer arises from the antibonding interaction of the a_{1u} orbitals of the three π orbitals, and the Nc ring has the largest MO coefficients. In contrast to the HOMO, the Nc plane becomes a node in the case of HOMO-1, so that the interaction energy is considered to be small. The HOMO-2 should be composed primarily of OEP orbitals and thus stabilized because of the bonding interaction of the three chromophores. Similar MO interactions are present on the unoccupied MOs. This model predicts that the HOMO-LUMO energy splitting decreases with decreasing size of the central metal. The fact that Eu(Nc)(OEP)2 ($E_{1/2}$ = 0.184 V (vs SCE)) undergoes oxidation more readily than $Nd(Nc)(OEP)_2$ ($E_{1/2}$ = 0.300 V (vs SCE)) strongly indicates that our present view is rational [10]. According to the simple MO model, band **I** is attributed to a HOMO-LUMO transition which possesses the Q-band character of the Nc. From the peak positions, Bands **II** and **III** are assigned to a transition from HOMO-1 to LUMO+1 and a transition from HOMO-2 to LUMO+2, respectively (Fig. 13).

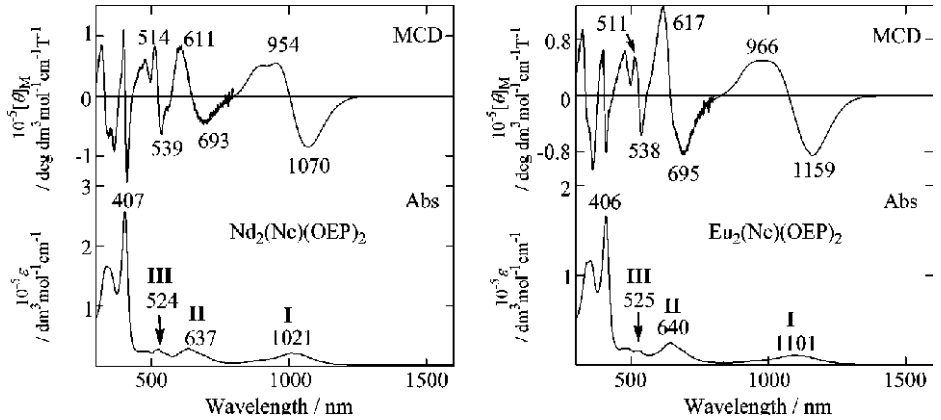

Fig. 12. Electronic absorption and MCD spectra of $M_2(Nc)(OEP)_2$ (M = Nd, Eu) recorded in $CHCl_3$ at room temperature

Рис. 12. Электронные спектры поглощения и МКД M_2 (Nc) $(OEP)_2$ (M = Nd, Eu), записанные в $CHCl_3$ при комнатной температуре

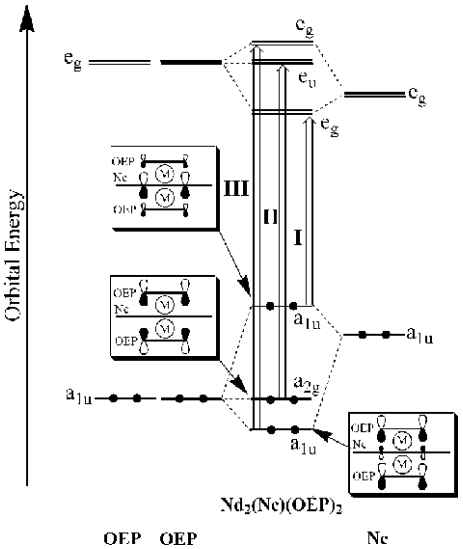

Fig. 13. Schematic representation of the frontier MO energy levels of the D_{4h} triple-decker, $M_2(Nc)(OEP)_2$. Simple MO models are drawn for the three occupied MOs

Рис. 13. Схематическое представление пограничных уровней энергии МО трехуровневый D_{4h}, M_2 (Nc) $(OEP)_2$. Простые модели МО нарисованы для трех занятых МО

The present study has demonstrated a readily accessible and intuitive MO model to rationalize the main features of the electronic structures of the naphthalocyanine-octaethylporphyrin (OEP) rare-earth sandwich complexes (M(Nc)(OEP), M = La, Nd, Eu, Dy, and Lu). To comprehensively understand the excited states, the MCD spectra of the dimer have been measured up to 2000 nm. By considering the observed MCD signals and the MO structure of the dimer, the two lowest near-IR absorption bands (Bands **I** and **II**) of the neutral form of M(Nc)(OEP) were assigned to the HOMO→SOMO and SOMO→LUMO transitions, respectively. The MO model could account for the systematic shifts of a series of lanthanide dimers observed for Bands **I** and **II**. The interaction between the monomeric MOs increases with decreasing size of central metal, resulting in a spectral blue-shift and red-shift corresponding to the HOMO→SOMO (Band **I**) and SOMO→LUMO transitions (Band **II**). The spectral changes on going from the neutral form to the reduced or oxidized forms were also successfully explained using the MO models: since the Nc-OEP distance decreases in the order of $[M(Nc)(OEP)]^-$ > $[M(Nc)(OEP)]$ > $[M(Nc)(OEP)]^+$, the bonding or antibonding interactions of the constituent monomeric MOs become larger in the same order. The DFT calculations agree well with the conceptual model presented here and succeeded in reproducing the experimental trends (i.e., the shift of the absorption band with ionic size of the rare-earth metal). This simple intuitive MO model was applied for the interpretation of the electronic absorption and MCD spectra of the OEP-Nc-OEP triple-decker systems ($M(Nc)(OEP)_2$, M = Eu, Nd), and succeeded in reasonably explaining the spectral shift with the size of the rare-earth metal and dispersion type Faraday A-term MCD curves. This study allows us to highlight the importance of bonding or antibonding MO interactions and the usefulness of MCD spectroscopy for understanding the electronic structures of heteroleptic sandwich species of porphyrinoids.

c) Optically Active Mixed Phthalocyaninato–Porphyrinato Rare-Earth Double-Decker Complexes: Synthesis, Spectroscopy, and Solvent-Dependent Molecular Conformations [15]

Over the past few decades, optically active porphyrin and phthalocyanine derivatives have also been intensively studied [16], however, chiral sandwich porphyrinato and phthalocyaninato metal complexes remain extremely rare to date. We report the

preparation and characterization of the first optically active mixed phthalocyaninato–porphyrinato rare-earth complexes [$M^{III}H\{Pc(OBNP)_2\}(TClPP)$] (M = Y (**1**), Eu (**2**) ; OBNP = binaphthylphthalocyanine, TClPP = *meso*-tetrakis(4-chlorophenyl)-porphyrinate; Scheme 3). To enhance the asymmetric perturbation to the tetrapyrrole chromophores in the sandwich-type mixed phthalocyaninato–porphyrinato rare-earth double-decker molecules through dipole–dipole interactions, aromatic chiral binaphthyl units were introduced onto the nonperipheral positions of the phthalocyanine ring. In addition to electronic absorption and MCD spectroscopy results, circular dichroism (CD) reveals different spectroscopic features of these mixed-ring rare-earth double-decker compounds in different solvents. On the basis of time-dependent density functional theory (TD-DFT) results on the yttrium species (*S*)-[$Y^{III}\{Pc(OBNP)_2\}(Por)$]- in terms of different rotation angles between the two macrocyclic ligands in the double-decker molecules, different electronic absorption and CD spectroscopic features of (*S*)-[$Y^{III}H\{Pc(OBNP)_2\}(TClPP)$] in DMF and $CHCl_3$ were well reproduced, which revealed the solvent-dependent nature of the mixed-ring rare-earth double-decker complexes on the molecular conformation.

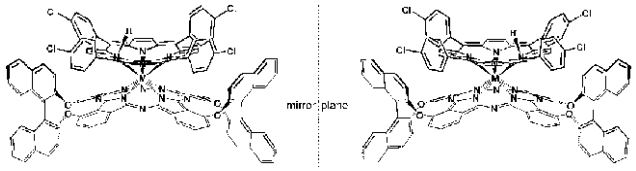

(S)-[$M^{III}H\{Pc(OBNP)_2\}(TClPP)$] (R)-[$M^{III}H\{Pc(OBNP)_2\}(TClPP)$]

Scheme 3. Schematic molecular structures of **1** and **2**

Схема 3. Схематичное строение молекул **1** и **2**

The fact that the electronic absorption spectra of mixed phthalocyaninato–porphyrinato rare-earth complexes, and other bis(tetrapyrrole)–rare-earth compounds, change depending on the solvent has puzzled chemists in this field for a long time [17]. Cofacial dimerization of the tetrapyrrole–metal double-decker compounds in solution, in a similar manner to planar, flat monomeric phthalocyanine compounds, was proposed to explain the spectroscopic change with solvent; however, this has never been verified. Here we reveal that the change in the optical spectroscopic spectra of mixed phthalocyaninato–porphyrinato rare-earth complexes with solvent (DMF and $CHCl_3$) is due to the change in the double-decker molecular conformation associated with different interactions between the double-decker and solvent molecules. This represents the first effort to understand the change in the optical spectra of bis(tetrapyrrole)–metal complexes with solvent.

Synthesis and characterization of [$M^{III}H\{(OBNP)2\}(TClPP)$] (M = Y (1) or Eu (2)): Phthalocyanine with aromatic chiral binaphthyl units at the nonperipheral positions ($H_2\{Pc(OBNP)_2\}$) were chosen to synthesize the target sandwich rare-earth complexes. However, efforts using $H_2\{Pc(OBNP)_2\}$ to synthesize both homoleptic and heteroleptic bis(phthalocyaninato)–rare-earth complexes failed. Surprisingly, reaction of $H_2\{Pc(OBNP)_2\}$ with the half-sandwich porphyrinato rare-earth complexes [M^{III}(acac)(TClPP)] (M = Y, Eu ; acac = acetylacetonate), generated *in situ* from $M(acac)_3 \cdot nH_2O$ and H_2(TClPP) in *n*-octanol at reflux led to the isolation of optically active protonated mixed phthalocyaninato–porphyrinato rare-earth double-deckers (*S*)- and (*R*)-[$M^{III}H\{Pc(OBNP)_2\}(TClPP)$] (M = Y (**1**) or Eu (**2**)) in good yields. Racemization of the Pc did not occur at temperatures over 180° under the reaction conditions. Yttrium compound **1** was EPR silent, which showed its diamagnetic property and revealed the protonated nature of these double-decker complexes.

Electronic absorption, MCD, and CD spectra of 1 and 2 recorded in DMF and $CHCl_3$: The electronic absorption, MCD, and CD spectra of **1** and **2** were recorded in DMF (Fig. 14. Both complexes **1** and **2** have five absorption bands in their electronic absorption spectra, a typical feature of the protonated mixed phthalocyaninato–porphyrinato rare-earth double-decker complexes. They display medium to strong phthalocyanine (338 nm) and porphyrin (419~424 nm) Soret bands and several Q bands in the region of 616 to 842 nm in the spectra recorded in DMF. The spectrum also displays a medium band at 485 to 488 nm. However, the absence of the characteristic near-IR absorption at around 1200 nm for the neutral species in the electronic absorption spectra of both compounds again indicates the protonated nature of these double-deckers [18]. Associated with absorption peaks, the MCD spectra apparently showed dispersion-type Faraday A terms, which suggested that these correspond to transitions to the almost degenerate excited states [11, 12, 19-21]. As shown in Fig. 14a, the optically pure isomers of both yttrium and europium compounds show perfect mirror-image CD spectra of each other in the whole spectral region. For both of the *S* isomers, the CD sign is positive between 370 and 420 nm and beyond approximately 630 nm, whereas the sign is negative between approximately 310 and 370 nm and 420 and 630 nm. Their CD intensities are $[\theta] = 0.5\times10^5$ to 6×10^5. The intense and sharp CD signal observed at 343 nm is characteristic of the CD of the monomeric binaphthyl-linked phthalocyanine [22].

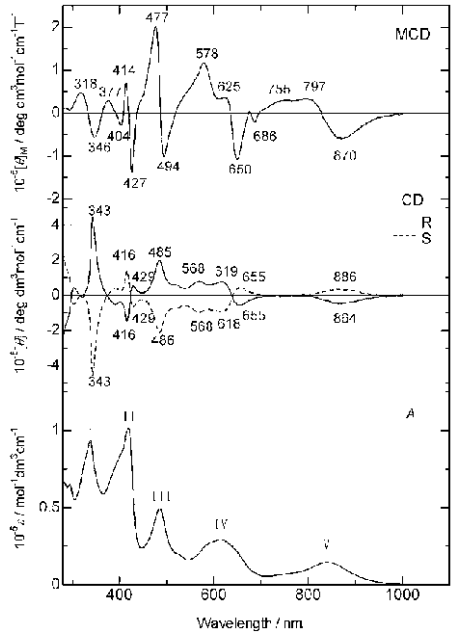

a

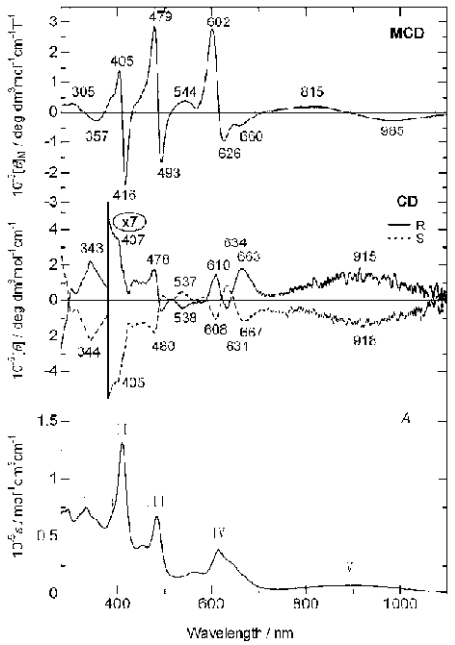

b

Fig. 14. Electronic absorption, MCD, and CD spectra of **1** measured in a) DMF and b) $CHCl_3$

Рис. 14. Электронные спектры поглощения, МКД и CD **1**, измеренные в a) ДМФА и b) $CHCl_3$

The electronic absorption spectra for these two protonated mixed-ring double-decker complexes $[M^{III}H\{Pc(OBNP)_2\}(TClPP)]$ (M = Y, Eu) (**1**, **2**) change depending on the solvent. As shown in Fig. 14, despite the overall similar spectroscopic features, clear differences in the electronic absorption spectra of these two double-decker compounds recorded in $CHCl_3$ can be observed from those recorded in DMF. For example, both the Pc and porphyrin Soret bands of **1** and **2** shift from 338 and 420-424 nm in DMF to higher energy positions (333 and 410-415 nm) in $CHCl_3$. In contrast, the lowest-energy absorption band at 820 to 842 nm in DMF for **1** and **2** appears to become weaker and extends to longer wavelengths between 848-888 and 1100 nm in $CHCl_3$. Additionally, the broad absorption at 616-630 nm in DMF for **1** and **2** splits into two absorptions at 562-564 and 615 nm in $CHCl_3$. Associated with the change in the electronic absorption spectra, pseudo-Faraday A terms corresponding to the porphyrin Soret band at 410-415 nm, the porphyrin Q band at 484 nm, and the absorption at 615 nm in the MCD spectra recorded in $CHCl_3$ become sharper than those in DMF. More importantly, corresponding with the changes in the electronic absorption and MCD spectra, the CD spectra of the optical isomers for both complexes, in particular the yttrium compound, are completely different from those recorded in DMF in shape and the intensity becomes much weaker (about one third of that in DMF; see Fig. 14). It should be noted that both of the (*S*)-isomers exhibited a negative CD signal for the lowest-energy transition, in contrast to the positive CD in DMF.

All of the results described above appear to suggest a change in the molecular conformation of mixed phthalocyaninato–porphyrinato rare-earth complexes upon changing the solvent from DMF to $CHCl_3$. This is confirmed by the fact that the electronic absorption spectra of double-deckers change with a set of isosbestic points along with changing the ratio of DMF and $CHCl_3$, but maintaining a constant sample concentration (Fig. 15). Cofacial dimerization of any sandwich-type bis(tetrapyrrole)–rare-earth double-decker compounds with two outwardly oriented tetrapyrrole ligands in the molecule through π–π interactions between two double-decker molecules has not been reported in any solution thus far. This, in combination with the fact that all of the absorption bands in **1** and **2** do not simultaneously take a blue- or redshift along with changing the solvent, such as from DMF to $CHCl_3$, indicates the transformation of non-aggregated molecular conformations in these two solvents.

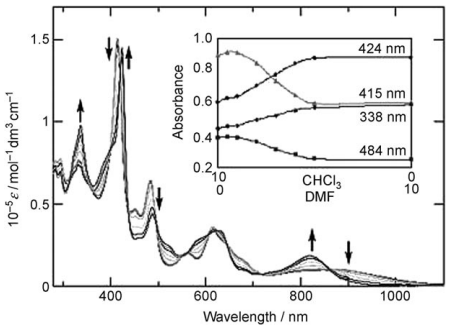

Fig. 15. Solvent effect on the electronic absorption spectra of **1**. The inset shows the change in the absorbance corresponding to the Soret bands

Рис. 15. Влияние растворителя на электронные спектры поглощения **1**. На вставке показано изменение поглощения, соответствующее полосам Соре

Electronic absorption and CD spectra of (*S*)-[Y^{III}{Pc(OBNP)$_2$}(TClPP)]$^-$ on the basis of TD-DFT calculations: On the basis of the experimental results described above, the change in the electronic absorption, MCD, and CD spectra of **1** and **2** is ascribed to the transformation of non-aggregated double-decker molecular conformations upon changing the solvent from DMF to $CHCl_3$. To get an insight into the relationship between the molecular conformation and the optical spectra of these double-decker compounds, TD-DFT calculations were carried out on the electronic absorption and CD spectroscopic properties of the yttrium species. Note that for economic reasons and to simplify the calculations, calculations on the spectra were actually carried on the anionic form of the yttrium double-decker [Y^{III}{Pc(OBNP)$_2$}(TClPP)]$^-$ or even [Y^{III}{Pc(OBNP)$_2$}(Por)]$^-$ (Por = porphyrinate, which is obtained from TClPP by removing the four chlorophenyl groups) instead of the protonated species [Y^{III}H{Pc(OBNP)$_2$}(TClPP)]. This is actually rationalized by assuming that the protonated mixed phthalocyaninato–porphyrinato rare-earth complexes have almost the same electronic absorption spectra as their anionic counterparts. Fig. 16 shows the optimized structure of (*S*)-[Y^{III}{(OBNP)$_2$}(TClPP)]$^-$ obtained at the B3LYP/LANL2DZ level. Accordingly, the two macrocycles in this molecule are rotated from the staggered position by about 13° with a ring-to-ring separation of approximately 2.818 Å between the plane that consists of four pyrrole nitrogen atoms and another that contains four isoindole nitrogen atoms. This value is in accordance with that found experimentally for [Y^{III}H{Pc(α-OC_5H_{11})$_4$}(TClPP)] (2.800 Å) [23]. It is worth noting that, in accordance with the experimental findings [23], both the Pc and porphyrin ligands are revealed to bend significantly out from the double-decker molecule. This gives further support for excluding the formation of a dimer of double-decker complexes through π–π interactions between two double-decker molecules.

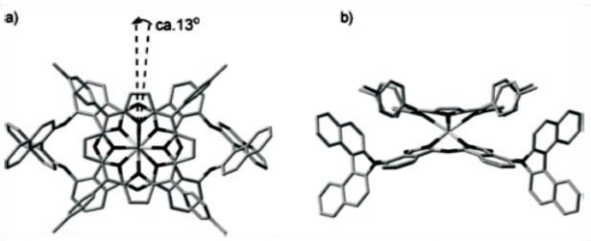

Fig. 16. The top (a) and side (b) views of the optimized structure of (*S*)-[Y^{III}{Pc(OBNP)$_2$}(TClPP)]$^-$. Hydrogen atoms are omitted for clarity

Рис. 16. Вид сверху (а) и сбоку (b) оптимизированной структуры (*S*) - [Y^{III} {Pc (OBNP)$_2$} (TClPP)] -. Атомы водорода опущены для ясности

To further simplify the calculations, the four chlorophenyl groups were removed from the TClPP ligand in the optimized structure during TD-DFT calculations of the spectroscopic properties of the yttrium double-decker compound. The electronic absorption spectrum together with the CD spectrum for (*S*)-[Y^{III}{Pc(OBNP)$_2$}(Por)]$^-$ was obtained on the basis of these calculations. Fig. 17 shows the simulated absorption and CD spectra of (*S*)-[Y^{III}{Pc(OBNP)$_2$}(Por)]$^-$. It is seen that the simulated electronic absorption and CD spectra of (*S*)-[Y^{III}{Pc (OBNP)$_2$}(Por)]$^-$ approximately reproduce the observed spectra of (*S*)-[Y^{III}H{Pc(OBNP)$_2$}(TClPP)] in DMF. The almost degenerate LUMO (LUMO+1) or LUMO+2 (LUMO+3) orbitals for (*S*)-[Y^{III}{Pc(OBNP)$_2$}(Por)]$^-$ are responsible for the observation of the pseudo A term for almost all of the electronic transitions. Comparison between the experimental and computational results renders it possible to assign the bands to those mainly associated with the Pc Soret, porphyrin Soret, porphyrin Q, charge-transfer (CT), and Pc Q transitions. The CD sign and relative intensity of these bands in the calculated spectra of (*S*)-[Y^{III}{Pc(OBNP)$_2$}(Por)]$^-$ are in excellent agreement with the observed CD signals for (*S*)-[Y^{III}H{Pc(OBNP)$_2$}(TClPP)] in the whole spectral region, which suggests that the present double-decker system, (*S*)-[Y^{III}H{Pc(OBNP)$_2$}(TClPP)], in DMF preferentially adopts a right-handed helical geometry (α = 13°) with respect to the staggered conformation (α = 0°).

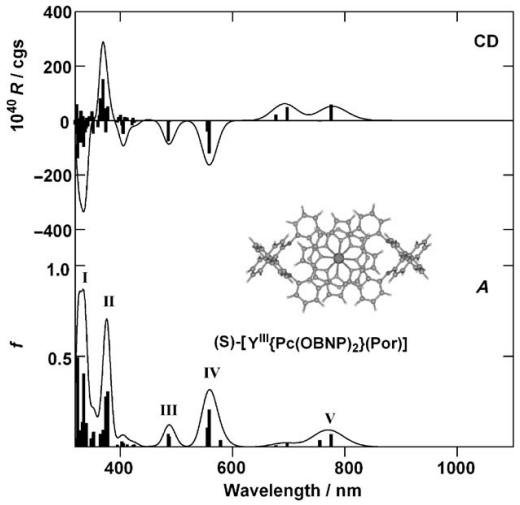

Fig. 17. Simulated electronic absorption and CD spectra of (*S*)-[Y^{III}{Pc(OBNP)$_2$}(Por)]$^-$ with the rotation angle of 13°. Gaussian bands with half-bandwidths of 1000 cm^{-1} were used

Рис. 17. Имитация электронных спектров поглощения и КД (*S*) - [Y^{III} {Pc (OBNP)$_2$} (Por)]$^-$ с углом поворота 13 °. Использовались полосы Гаусса с полуширинами 1000 см$^{-1}$

On the basis of single-crystal molecular structure investigations over a large number of bis(tetra-

pyrrole)–metal complexes [18, 23, 24], double-decker molecules with two parallel tetrapyrrole ligands connected by a large-radius metal cation can change their molecular conformation only in terms of the twist angle and ring-to-ring distance. The twist angle, θ, for bis(tetrapyrrole)–metal complexes is usually defined as the rotation angle of one macrocycle away from the eclipsed conformation of the two macrocycles. However, in the present study, the rotation angle (α) employed for the anionic mixed phthalocyaninato–porphyrinato yttrium complex is different from θ, the value of which is actually the difference between θ and an angle of 45°, that is, $\alpha = \theta - 45°$. Furthermore, it is reasonable to consider that changes in the protonated mixed-ring double-decker molecules connected by the same yttrium or europium ion in **1** and **2** should only occur in the rotation angle with the ring-to-ring distance remaining unchanged upon changing the solvent from DMF to $CHCl_3$ or *vice versa*. As a consequence, to understand the significant change in the CD spectra of complexes **1** and **2** upon changing the solvent from DMF to $CHCl_3$, the CD signal for the lowest-energy transition of (*S*)-$[Y^{III}\{Pc(OBNP)_2\}(Por)]^-$ together with the relative energy for this molecule was calculated by changing the rotation angle of α in the range from 13 to -2° with a ring-to-ring separation of 2.818 Å. It is worth noting that such a rotation angle range from 13 to -2° was also selected on the basis of single-crystal molecular structure investigation results [24], which reveal the skew angle for most bis(tetrapyrrole)–rare-earth complexes in the range between 35 and 45°, which corresponds to a range of 10 to 0° for the rotation angle of α.

As shown in Fig. 18, along with the decrease in the rotation angle, the CD signal for the lowest-energy transition of (*S*)-$[Y^{III}\{Pc(OBNP)_2\}(Por)]^-$ gradually changes its sign from positive to negative when α is less than 2°. Nevertheless, when the rotation angle becomes 0°, the intensity of the CD signal with negative sign corresponds to approximately a quarter of that for α = 13°. This observation is in good agreement with the experimental result of (*S*)-$[Y^{III}H\{Pc(OBNP)_2\}(TClPP)]$ recorded in $CHCl_3$ (see above).

As expected, the calculated relative energy (E_{rel}) of (*S*)-$[Y^{III}\{Pc(OBNP)_2\}(Por)]^-$ increases with decreasing the twist angle α as a result of the steric repulsion between the peripheral substituents of two macrocycles. In particular, this compound appears to be unrealistic in terms of energy after the rotation angle decreases to less than -2°. On the basis of these results, the electronic absorption and CD spectra of (*S*)-$[Y^{III}\{Pc(OBNP)_2\}(Por)]^-$ with $\alpha = 0°$ were calculated at the level of B3LYP/LANL2DZ (see Fig. 19). As can be found, both the calculated electronic absorption and in particular the CD properties reproduce the experimental spectra of (*S*)-$[Y^{III}H\{Pc(OBNP)_2\}(TClPP)]$ in $CHCl_3$, which suggests a fully staggered molecular structure with a rotation angle of 0° employed by the compound $[Y^{III}H\{Pc(OBNP)_2\}(TClPP)]$ in $CHCl_3$.

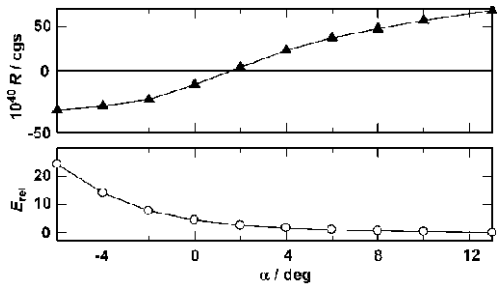

Fig. 18. a) Plot of the calculated CD intensity for the lowest-energy transition. b) Plot of E_{rel} [kcal mol^{-1}] of (*S*)-$[Y^{III}\{Pc(OBNP)_2\}(Por)]^-$ as a function of α

Рис. 18. а) График рассчитанной интенсивности КД для перехода с наименьшей энергией. b) График E_{rel} [ккал $моль^{-1}$] of (*S*) - $[Y^{III}\{Pc(OBNP)_2\}(Por)]^-$ как функция α

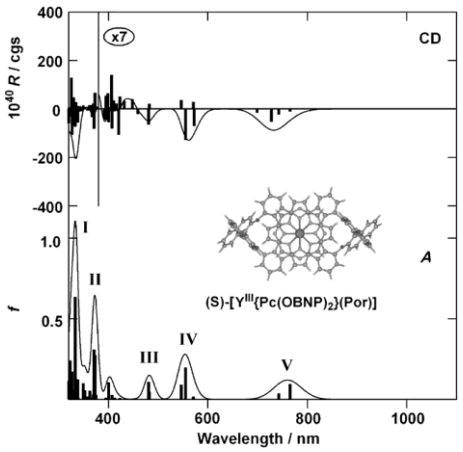

Fig. 19. Simulated electronic absorption and CD spectra of (*S*)-$[Y^{III}\{Pc(OBNP)_2\}(Por)]^-$ with a rotation angle of 0°. Gaussian bands with half-bandwidths of 1000 cm^{-1} were used

Рис. 19. Имитация электронных спектров поглощения и КД спектра (*S*) - $[Y^{III}\{Pc(OBNP)_2\}(Por)]$ - с углом поворота 0 °. Использовались полосы Гаусса с полуширинами 1000 $см^{-1}$

In summary, we have prepared the first optically active mixed phthalocyaninato–porphyrinato rare-earth double-decker complexes **1** and **2**. Electronic absorption, MCD, and CD spectroscopic properties in different solvents reveal their solvent-dependent molecular conformations. Theoretical calculation results on their electronic absorption and, in particular, their CD spectra by using the TD-DFT method reproduce the change in the optical properties in terms of changes in the twist angle of double-decker molecules, which confirms the non-aggregated molecular conformation change of mixed phthalocyaninato–porphyrinato rare-earth double-decker complexes along with changing the solvent from DMF to $CHCl_3$.

d) *anti*-[2.2](1,4)Phthalocyaninophane: Spectroscopic Evidence for Transannular Interaction in the Excited States [25]

A novel type of bisphthalocyanines, *anti*-[2.2](1,4)-phthalocyaninophanes (**1Zn** and **1Cu**), in which two Pc units are linked by ethano bridges at the para positions, was reported to create a [2.2]-*para*-cyclophane moiety (Fig. 20). The cyclophane framework could allow for a well-defined slipped-stack arrangement of the two Pc units. Construction of this kind of a slipped-stack dimer has been stimulated by the fact that the special pair and antenna subunits in photosynthetic light-harvesting antenna consisting of bacteriochlorophyll dimers have a similar spatial arrangement to fine-tune the electronic excited states [26], and that the fluorescence properties of a Pc chromophore preserve, which is in contrast to non-fluorescent Pc oligomers with face-to-face geometry [27].

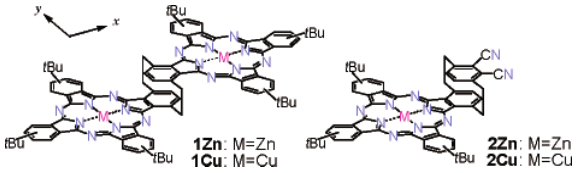

Fig. 20. Structures of phthalocyaninophanes
Рис. 20. Структуры фталоцианинофанов

The *anti*-[2.2](1,4)-zinc(II)-9(10),16(17),23(24)-tri-*tert*-butylphthalocyaninophane (**1Zn**) was synthesized from [2.2]paracyclophane in three steps. The *anti*-[2.2](3,6)-phthalonitrilo(1,4)zinc(II)-9(10),16(17),23(24)-tri-*tert*-butylphthalocyaninophane (**2Zn**) was also obtained in the synthetic procedure. The Cu complexes (**1Cu** and **2Cu**) were synthesized similarly to the Zn complexes. Fig. 21 shows experimental and calculated spectra of **1Zn**, **2Zn**, and reference zinc(II) tetra-*tert*-butylated Pc (**3Zn**). The 678 nm absorption band of **3Zn** splits into two well-resolved bands (683 and 706 nm) in the case of **2Zn**. The splitting of the Q-band appears to be similar to that of conventional low- symmetrical Pc derivatives reported previously [28].

In contrast, **1Zn** exhibited significantly split and red-shifted absorption bands, observed at 753 and 690 nm. It should be noted that, when compared to the dimeric Pcs with a similar geometrical arrangement, the lowest-energy Q-band position of the dimer lies midway between those of the Pc dimer without π-conjugation (*J*-type Pc dimer, 700 nm) [29] and π-conjugated planar Pc dimer (852 nm) [30]. The MCD signals of **1Zn** and **2Zn** associated with the two lowest-energy transitions have negative {$[\theta]_M$ = -6.23×10^5 (**1Zn**), -1.05×10^6 (**2Zn**)} and positive signs {$[\theta]_M$ = 7.52×10^5 (**1Zn**), 7.21×10^5 (**2Zn**)}, respectively. The Q absorption peak positions are almost the same as the observed trough and peak, so that these signals are assigned to coupled Faraday B terms, which arise from magnetically induced mixing of nondegenerate excited states [11, 12, 19, 21]. Since the spectral pattern of **1Zn** was unchanged upon addition of pyridine and a linear relationship between absorbance and concentration was confirmed in Beer's law experiments, aggregation behavior should be negligible under the experimental conditions. The spectroscopic properties of the Cu complexes (**1Cu** and **2Cu**) were almost identical to those of the Zn complexes. From these spectroscopic data, it is evident that significant through-space π-π interactions are involved in the excited singlet states of the present system.

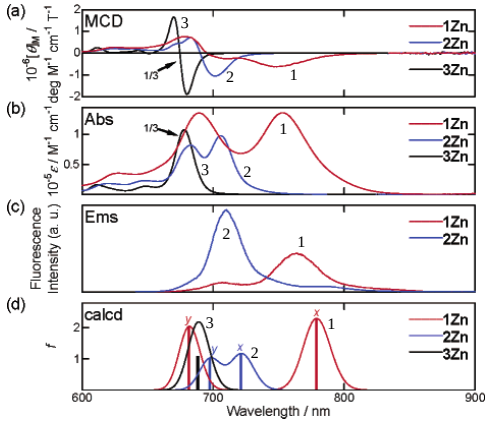

Fig. 21. MCD (a), absorption (b), and fluorescence (c) spectra of **1Zn** (1), **2Zn** (2), and **3Zn** (3) in benzene. ZINDO/S calculations (d). Gaussian bands with half-bandwidth of 400 cm^{-1} were used; x and y indicate transition polarizations
Рис. 21. Спектры МКД (а), поглощения (б) и флуоресценции (с) **1Zn** (1), **2Zn** (2) и **3Zn** (3) в бензоле. Расчеты ZINDO/ S (d). Использовались полосы Гаусса с полушириной 400 $см^{-1}$; x и y обозначают переходные поляризации

According to the B3LYP/6-31G* optimized structures, the average distance between the facing benzene planes is 2.98 Å. The geometrical parameters of the cyclophane moiety of **1Zn** and **2Zn** are close to those of [2.2]paracyclophane calculated using the B3LYP functional, suggesting that a considerable electron exchange within the π units should be taken into account [31]. The calculated spectral features (ZINDO/S) are in good agreement with the experimental spectra. It is clearly seen from Fig. 22 that the MOs of **1Zn** consist of linear combinations of the monomeric MOs. The lowest and second lowest energy absorption bands of both **1Zn** and **2Zn** can be attributed to long- and short-axis polarized Q transitions, respectively, since these transitions were formed predominantly through combinations of MOs derived from Gouterman's orbitals [7]. These results agree with the observed coupled Faraday B terms since transitions of

different polarizations generally have differently signed MCD signals [19, 21]. In view of the assignment of the polarization of the Q-bands, the MO calculation is consistent with Kasha's exciton coupling theory [32].

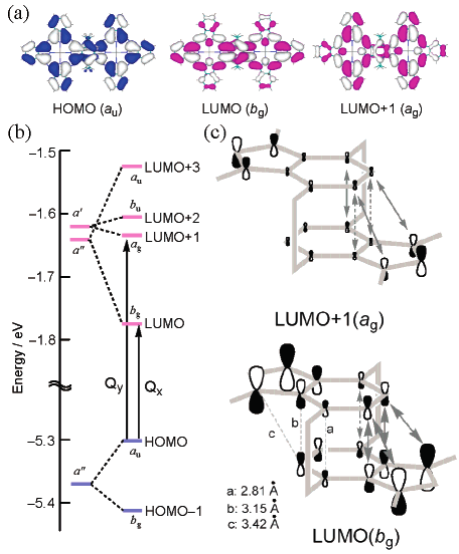

Fig. 22. (a) Frontier MOs of the B3LYP-optimized **1Zn**. (b) Energy correlation diagram of zinc dimethyl Pc (left) and **1Zn** (right). (c) Schematic representation of the origin of the π-π interaction. The relative π orbital size is based on the CI calculations. Bonding and antibonding interactions are indicated by solid and dotted arrows, respectively

Рис. 22. (а) Пограничные МО оптимизированного B3LYP **1Zn**. (б) Диаграмма энергетической корреляции диметил Pc-цинка (слева) и **1Zn** (справа). (с) Схематическое представление происхождения π-π-взаимодействия. Относительный размер π-орбитали основан на расчетах CI. Связывающие и антисвязывающие взаимодействия обозначены сплошной и пунктирной стрелками, соответственно

The origin of the spectral features of **1Zn** was rationalized as shown in Fig. 22b. The HOMO and LUMO are destabilized and stabilized, respectively, compared with a corresponding Pc monomer due to the significant orbital interactions, which leads to the spectral red shift (Q_x). Since the stabilization of the LUMO+1 is modest, the energy difference between the LUMO and LUMO+1 becomes large, which results in the marked Q_x-Q_y splitting. The orbital interaction energies of **1Zn** are calculated to lie midway between those of the corresponding Pc dimer with and without π-conjugation. Fig. 22c illustrates a schematic representation of the π orbitals of the cyclophane moiety in the LUMO and LUMO+1. In the case of the LUMO, bonding interactions between the benzene π orbitals on one Pc unit and the pyrrole π orbitals on the other Pc unit contribute to the stabilization of the LUMO energy, although the interaction between the π orbitals on the nearest carbons is slightly antibonding. In contrast, since the relative size of the π orbitals on the cyclophane moiety of the LUMO+1 is considerably small, the through-space π-π interactions between the benzene and pyrrole units are weak, which results in moderate stabilization of the LUMO+1. The small Q-band splitting observed for **2Zn** can also be rationalized by considering the relative size of the π orbitals in the cyclophane moiety.

In summary, we have demonstrated the design and synthesis of a novel bisphthalocyanine system (**1Zn** and **1Cu**) that exhibited significantly split and red-shifted absorption in the near-IR region. It was found that **1Zn** maintained the fluorescence properties of Pcs. The MO model analysis provides a clear-cut picture for the nature of the electronic communication between the two Pc chromophores, which could offer a new approach for understanding transannular interactions of cyclophanes. In addition, since the phthalocyaninophanes can mimic the slipped-stack arrangement with significant interchromophore coupling, the present system has potential application as a novel model of the special pair and subunits in photosynthetic systems.

e) Cyclophanes Containing Bowl-Shaped Aromatic Chromophores: Three Isomers of *anti*-[2.2](1,4)Subphthalocyaninophane [33]

Owing to the small distance between the two constituent benzene units, paracyclophane is generally considered to be one of the most suitable cyclophanes for investigating the transannular interaction. To our knowledge, all previously reported cyclophane derivatives containing aromatic chromophores consist of flat π-conjugated molecules, and no species consisting of curved aromatic molecules has been described. Accordingly, we reported the synthesis and characterization of [2.2]paracyclophane derivatives containing two bowl-shaped aromatic boron subphthalocyanines (SubPcs), which are contracted analogues of phthalocyanines that contain three isoindole rings. The combination of two SubPc units with [2.2]paracyclophane produces three isomers, which differ in the orientation of the convex and concave surfaces of the SubPc units with respect to the paracyclophane moiety. The difference in the electronic communication between the curved conjugated systems through the cyclophane moiety can be detected as changes in spectroscopic properties. These differences in the structure and properties of [2.2]paracyclophane derivatives with curved chromophores were described.

anti-[2.2](1,4)Subphthalocyaninophane and its monomer species, *anti*-[2.2](3,6)phthalonitrilo-subphthalocyaninophane, were synthesized by simply treating 4,5,12,13-tetracyano [2.2]*para*cyclophane [25] with an excess of tetrafluorophthalonitrile in the presence of boron trichloride in *p*-xylene at reflux (Scheme 4). The crude product was treated with an excess of

phenol to prevent adsorption and axial-ligand substitution during purification by silica-gel column chromatography. As expected, as a result of the bowl shape of SubPc, three isomers of *anti*-[2.2](1,4)subphthalocyaninophane (concave–concave (**CC**), convex–concave (**CV**), and convex-convex (**VV**) isomers) and two isomers of its monomer species (*endo* (**endo**) and *exo* (**exo**) isomers) were obtained, along with perfluorinated SubPc as the major product. The yields of the dimer species were 2.2 % for **CC**, 4.8 % for **CV**, and 15.7% for **VV**, and those of the monomer species were 1.5 % for **endo** and 5.1 % for **exo**. The higher yields of **VV** and **exo** as compared to those of **CC** and **endo** are indicative of preferential formation of the sterically less hindered compounds with the adjacent moiety residing on the **exo** side of the SubPc unit.

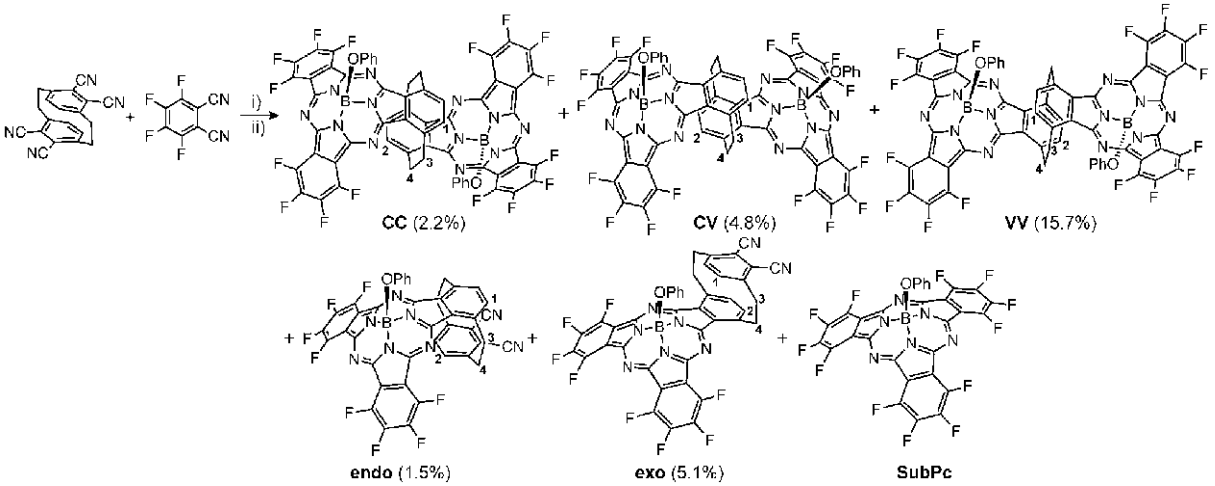

Scheme 4. Synthesis of *anti*-[2.2](1,4)subphthalocyaninophane and *anti*-[2.2](3,6)phthalonitrilosubphthalocyaninophane. Reaction conditions: i) BCl_3, p-xylene, reflux; ii) phenol, 125°C

Схема 4. Синтез *анти*-[2.2] (1,4) субфталоцианинофана и *анти*-[2.2] (3,6) фталонитрилосубфталоцианинофана. Условия реакции: i) BCl_3, п-ксилол, дефлегмация; ii) фенол, 125 ° C

The crystal structures of **CC** and **VV** were elucidated by X-ray crystallographic analysis of single crystals obtained by the slow diffusion of hexane into solutions of these dimer species in $CHCl_3$. It was found that the SubPc units each reside on the *endo* and *exo* surface of the other SubPc unit in **CC** and **VV**, respectively (Fig. 23). A boron atom lies above the plane defined by the three coordinating nitrogen atoms by 0.64 Å in **CC** and 0.63 Å in **VV**; these distances are within the range observed for regular SubPcs (0.59-0.66 Å). The distance between the bridge-head carbon atoms is 2.75 Å for **CC** and 2.76 Å for **VV**. Owing to the short distance of the ethylene bridge, the two bridged benzene rings are deformed, and have shallow V-shaped structures. The distance between the mean planes of the cyclophane benzene rings is 2.98 Å for **CC** and 2.91 Å for **VV**. The dihedral angle between these mean planes and the mean plane of the four ethylene carbon atoms is 78° for **CC** and 73° for **VV** (Fig. 23). These angles indicate that the cyclophane unit adopts a slip-stacked conformation, which is in clear contrast to the perpendicular orientation of the two planes in the parent [2.2]paracyclophane [34]. Although we could not obtain a suitable single crystal for structural analysis, the remaining dimer species was assigned as the convex–concave isomer (**CV**). Its structure was supported by ^{1}H NMR spectroscopy.

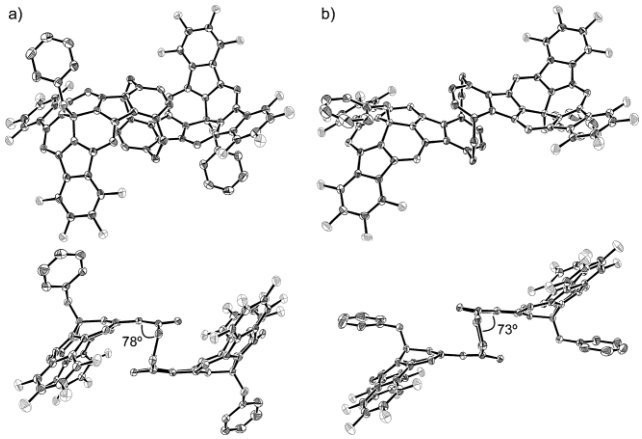

Fig. 23. X-ray crystal structures of ability level. Hydrogen atoms were omitted for clarity) **CC** and b) **VV** (top: top view, bottom: side view). The thermal ellipsoids were scaled to the 50 % probability level

Рис. 23. Рентгенокристаллические структуры уровня способности. Атомы водорода были опущены для ясности) **CC** и b) **VV** (сверху: вид сверху, снизу: вид сбоку). Термальные эллипсоиды были масштабированы до 50%

In the ^{1}H NMR spectra, the chemical shifts of the cyclophane hydrogen atoms unambiguously reflect the structural features of these cyclophane-containing SubPcs (Fig. 24). With respect to the benzene hydrogen atoms of unsubstituted [2.2]paracyclophane at 6.48 ppm, those of **CC** exhibited a significant upfield shift by 3.92 ppm to 2.54 ppm, whereas the upfield

shift observed for **VV** was marginal, at only 0.03 ppm. Owing to their presence on both the *endo* and *exo* sides, the signals of the cyclophane hydrogen atoms appeared at 6.48 and 2.38 ppm in the case of **CV**. On the basis of this assignment, the monomer species **endo** and **exo,** which exhibited a proton signal at 2.32 and 6.09 ppm, respectively, could be assigned as the **endo** and **exo** isomers. These experimental chemical shifts were reproduced well by DFT calculations. The cyclophane bridging also affected the chemical shifts of the axial phenoxy ligand. The dwnfield shifts observed for the axial ligand on the SubPc unit with *exo* bridging can be explained by the deshielding effect of the diatropic ring current of the benzene ring or the subphthalocyanine moiety on the *exo* side.

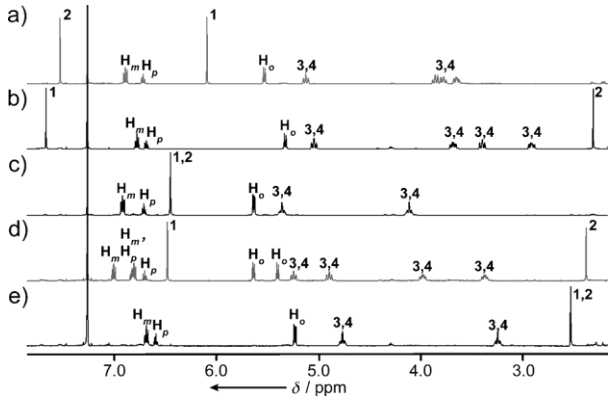

Fig. 24. ^{1}H NMR spectra of a) **exo**, b) **endo**, c) **VV**, d) **CV**, and e) **CC** in $CDCl_3$. The assignment follows the numbering scheme in Scheme 4. $\mathbf{H_o}$, $\mathbf{H_m}$, and $\mathbf{H_p}$ denote hydrogen atoms at the *ortho*, *meta*, and *para* positions of the axial phenyl substituents

Рис. 24. ^{1}H ЯМР спектры a) **экзо**, b) **эндо**, c) **VV**, d) **CV** и e) **CC** в $CDCl_3$. Отнесение следует схеме нумерации на Схеме 4. $\mathbf{H_o}$, $\mathbf{H_m}$ и $\mathbf{H_p}$ обозначают атомы водорода в *орто*-, *мета*- и *пара*-положениях аксиальных фенильных заместителей

Despite the difference in the distance from the center of the SubPc unit, the clear upfield shift of the *endo* cyclophane hydrogen atoms indicated a more significant shielding effect of the diatropic ring current on the *endo* side than on the *exo* side. However, dynamic molecular motions of the probing moieties are inherent to these systems, such as rotation of the Cp* ligand. The current cyclophane-containing SubPc systems are the first structurally rigid probes for the diatropic ring-current effect arising from the bowl-shaped aromatic molecules.

UV/Vis absorption and MCD spectroscopic measurements revealed the extent of the perturbation by annulation of the cyclophane unit and the through-space interaction based on the transannular effect. In comparison with regular SubPcs, the dimer species showed dramatic spectral changes on going from **CC** to **CV** and to **VV** (Fig. 25 a-c). The Q-band spectral shape of **CC** was similar to those of regular SubPcs with only a redshift by approximately 20 nm. Without any change in the Q-band position, **CV** and **VV** exhibited broadening and a decrease in intensity of the Q band, and in the case of **VV**, the Q-band absorption split into two peaks at 617 and 593 nm. Because the molecular symmetries of these SubPcs are lower than C_3, all of the MCD spectra in the Q-band region consist of a superimposition of Faraday B terms with a minus-to-plus sequence on ascending energy, which resulted in pseudo Faraday A terms, except for **VV** [11, 19, 35]. Owing to the splitting of the Q band, **VV** exhibited clear B terms at 608 and 585 nm. In contrast to the dependence of the absorption spectral morphologies on the manner of bridging of the two SubPc units in the case of the dimers, both of the monomer species, **exo** and **endo**, exhibited similar absorption and MCD spectra with respect to those of regular SubPcs, although the Q band was slightly shifted to the red by approximately 15 nm (Fig. 25 d,e). All compounds retained the fluorescence properties of SubPc analogues and exhibited intense emission with fluorescence quantum yields of 0.15 for **CC** and 0.16 for both **CV** and **VV**. The redshift in fluorescence was of the order observed for the absorption spectra (**endo** : 596 nm, **exo** : 600 nm, **CC** : 607 nm, **CV**: 626 nm, **VV**: 641 nm).

To enhance our understanding of the perturbation caused by the annulation of the cyclophane unit for the monomer species and the cyclophane bridging for the dimer species, DFT and (TD) DFT calculations were carried out at the CAM-B3LYP/6-31G(d) level [36] by using model structures, in which the axial phenoxy ligands were replaced with chlorine atoms for simplicity. For comparison, a half structure of the dimer species (**M1**), in which two methylene substituents are replaced with two methyl substituents, was also calculated. The TDDFT calculations estimated that the Q bands mainly consist of transitions between the six frontier molecular orbitals (MOs), the HOMO-1 and HOMO, and the LUMO~LUMO+3, which are ascribed to products of linear combinations of the HOMO and the LUMO and LUMO+1 of **M1** (Fig. 26). In the case of the homo- and heterodimer systems of Pc, SubPc, and related analogues sharing π-conjugated aromatic rings, such as benzene, naphthalene, and anthracene [37-40], the frontier MOs are known to be similarly developed by linear combination of the frontier MOs of the corresponding monomer species. In this respect, the through-space expansion of the conjugated systems through the cyclophane bridge in the case of the current SubPc dimer species was supported in theory. In fact, a certain amount of the MO coefficient was observed between the benzene rings of the cyclophane unit for the LUMO+1 of **CC** and the LUMO of **CV** and **VV**.

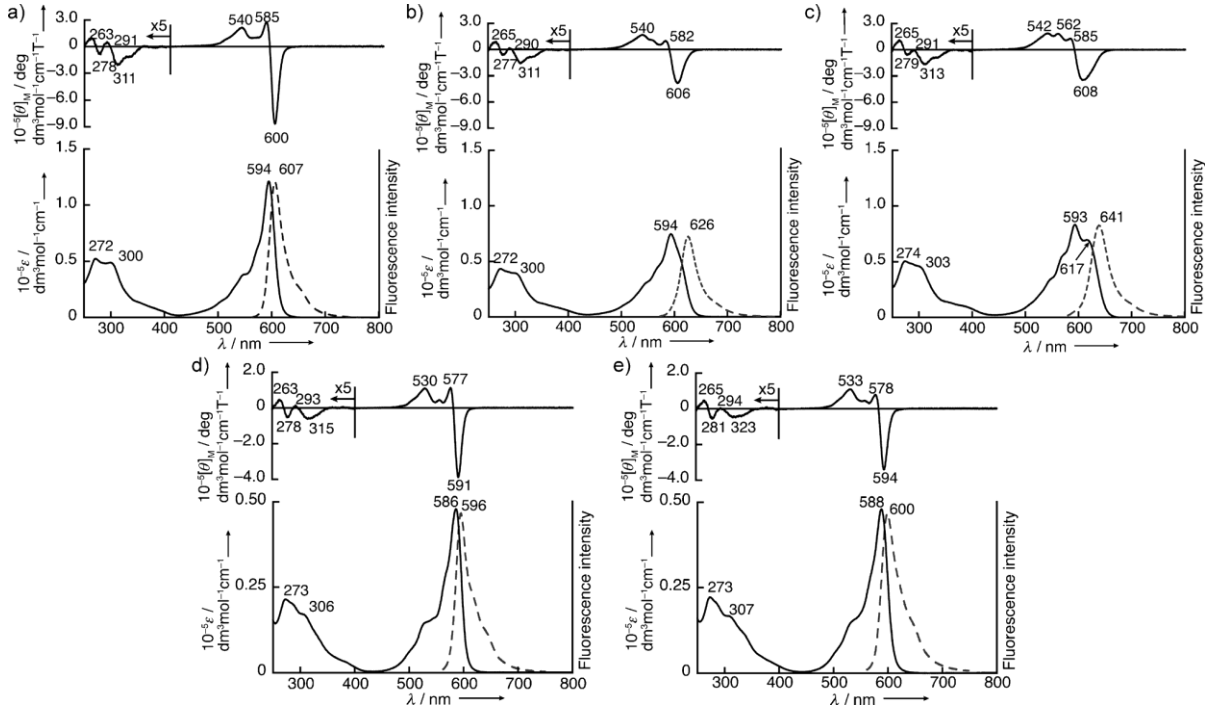

Fig. 25. UV/Vis absorption (bottom, solid line), MCD (top), and fluorescence spectra (bottom, dashed line) of a) **CC**, b) **CV**, c) **VV**, d) **endo**, and e) **exo** in $CHCl_3$

Рис. 25. УФ / Vis поглощение (внизу, сплошная линия), МКД (вверху) и спектры флуоресценции (внизу, пунктирная линия) a) **CC**, b) **CV**, c) **VV**, d) **endo** и e) **exo** в $CHCl_3$

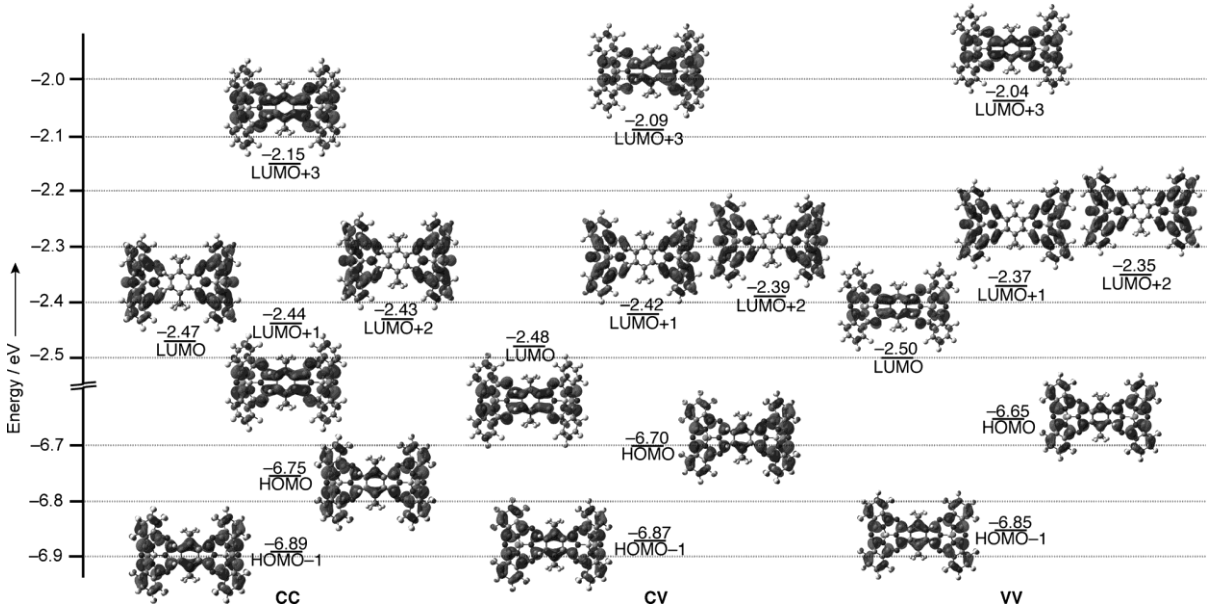

Fig. 26. Partial MO diagrams derived from CAM-B3LYP/6-31G(d) level DFT calculations of *anti*-[2.2](1,4)subphthalocyaninophane **CC** (left), **CV** (middle), and **VV** (right)

Рис. 26. Парциальные диаграммы MO, полученные из расчетов DFT уровня CAM-B3LYP / 6-31G (d) для *анти*-[2.2] (1,4) суб-фталоцианинофана **CC** (слева), **CV** (в центре) и **VV** (справа)

The TDDFT calculations reproduced well the observed redshift and broadening/splitting of the Q band on going from **CC** to **CV** and further to **VV**. Considering that the transition dipole moment of the lower-energy theoretical Q band lies along the long axis of the molecule, it can be concluded that changes in the molecular size and hence the size of the conjugated system along this axis in the order from **CC** to **CV** and to **VV** are related to the observed redshift of this band. This kind of conclusion could be reached in this study

for the first time by the preparation of cyclophane derivatives containing curved conjugated systems. Although the change in the Q-band position of the monomer species was very small (**endo**: 586 nm, **exo**: 588 nm), it can similarly be explained by a slight elongation of the conjugated system along the long molecular axis from **endo** to **exo**.

In summary, we have succeeded in designing, synthesizing, and separating three isomers of *anti*-[2.2]-(1,4)subphthalocyaninophane and two isomers of *anti*-[2.2]- (3,6)phthalonitrilosubphthalocyaninophane, in which the transannular interaction between the two bowl-shaped π-conjugated systems was investigated. The ^{1}H NMR spectra of these compounds unambiguously unveiled completely different environments on the *endo* and *exo* sides of the SubPc units. The broadening, redshift, and splitting observed in the Q band region of the absorption spectra of these compounds were reproduced well and explained by theoretical calculations.

3-2. Planar (Side-by-Side) Types

a) A zinc gable phthalocyanine and a derived planar bis-phthalocyanine containing a shared anthracene unit [40]

As planar Pc dimers, Leznoff was the first to report Pcs sharing a common benzene ring [41]. Since then, more than 20 papers describing planar Pc dimers and oligomers have been published. However, the effect of increasing Pc–Pc distance has not yet been examined. Accordingly, we describe the synthesis and spectroscopic (electronic absorption, fluorescence, and MCD) properties of the dizinc derivative of the gable-type metal-free Pc (ZnGPc (**1**)) and the derived planar Pc dimer (bis-ZnPc (**2**)) containing a shared anthracene ring which was obtained by heat treatment of ZnGPc (**1**). These two compounds are spectroscopically interesting, in that the Pc–Pc distance in (**2**) is much longer than those reported to date, and that the line connecting the two Pc units of (**1**) is folded while two lines normal to it through the Pcs of (**1**) are parallel to each other. As will be shown here, the Q band of the planar Pc in the present study appears different from that of the control monomeric Pc, and these characteristics are clearly interpreted with the help of molecular orbital (MO) calculations [42].

At first, metal-free gable Pc (GPc) was obtained by cross condensation using 2,3,6,7-tetracyano-9,10,11,12,13,14-hexahydrofuranothracene and *tert*-butylphthalonitrile in the presence of lithium alkoxide. Since the interpretation of spectra is easier for metalated species from the standpoint of molecular symmetry, we changed metal-free GPc to its Zn complex by reacting with $Zn(OAc)_2$ in dichloroethane–ethanol (3:2 v/v) under reflux for 12 hours in the dark. ZnGPc (**1**), thus obtained was then transformed into a planar Pc dimer by heat treatment, as reported for the formation of planar porphyrin dimers by Ono et al. [43]. Here, ^{1}H NMR signals originating from the gable moiety disappeared to produce an anthracene molecule, so that in the resulting dimer, two Pc units are connected by this anthracene molecule. The details of the synthesis are described in Scheme 5.

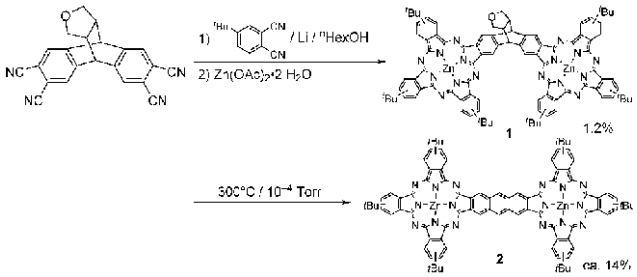

Scheme 5. Synthesis of the gable bis-Zn(II)Pc (**1**) and the conjugate planar bis-Zn(II)Pc (**2**)
Схема 5. Синтез фронтона бис-Zn (II) Pc (**1**) и сопряженного плоского бис-Zn (II) Pc (**2**)

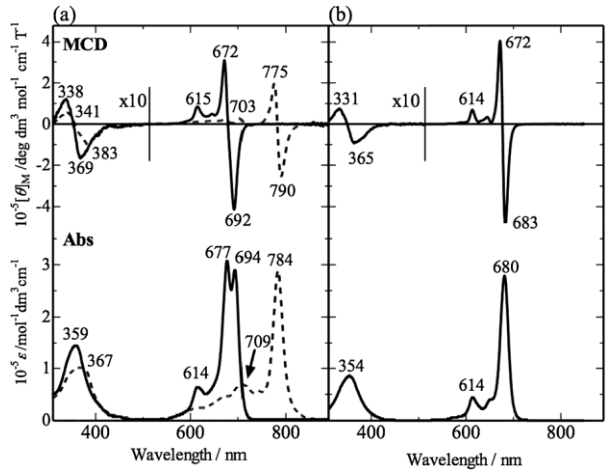

Fig. 27. Electronic absorption (bottom) and MCD spectra (top) in pyridine: (a) **1** (solid lines), **2** (broken lines), (b) **3**
Рис. 27. Спектры электронного поглощения (внизу) и МКД (вверху) в пиридине: (а) **1** (сплошные линии), **2** (пунктирные линии), (b) **3**

Fig. 27 shows the electronic and MCD spectra of **1**, **2** and tetra-*tert*-butylated ZnPc **3** [44]. The Q band of a typical monomeric Pc (D_{4h}), such as **3**, mainly consists of an $^1E_u \leftarrow {}^1A_{1g}$ transition [7, 19, 21], and comprises an unsplit Q absorption band, while the corresponding Faraday A MCD term (a derivative-shaped signal) at the center of the absorption band identifies a degenerate excited state (^1E_u). The Q band of C_{2v} symmetry **1** is split at 677 nm and 694 nm, and the MCD

spectrum shows coupled pairs of oppositely-signed Faraday B-term signals at 672 nm and 692 nm. For **2**, an apparently unsplit Q band appears at 784 nm in the near IR region, although **2** has approximate D_{2h} symmetry. The associated MCD spectrum is a pseudo Faraday A-term, since its trough and peak approximately correspond to the positions of the two absorption peaks.

The splitting of the Q band of compound **1** is quite easily explained by exciton coupling in an oblique two-chromophore system [32]. If we set the x-axis along the line connecting the two ZnPc units and the y-axis normal to the x-axis in the Pc plane, a transition along the x-axis shifts to longer wavelength, while that along the y-axis does not, so that the single Q band in D_{4h} symmetry **3** splits into two in C_{2v} symmetry **1**. However, the apparently unsplit Q band of **2** with D_{2h} symmetry was quite unexpected, particularly since it is known that the interaction of the two Pc units in this kind of planar system can be expressed as a linear combination of two almost independent Pc chromophores [37-39], by exciton coupling [32].

The calculated absorption spectra and molecular orbitals are shown in Fig. 28 and 29, respectively, with obtained data summarized in Table 3. From TD-DFT calculations at the B3LYP/631SVPs level, mutually perpendicularly polarized transitions of **1'** are calculated at 638, 607, 590 and 588 nm. From two e_g LUMOs and an a_{1u} HOMO of monomeric **3'**, four unoccupied orbitals and two occupied orbitals are produced as a linear combination of the LUMOs and HOMO, respectively. These results indicate that 318→319, 318→322, 317→319 and 317→322 are assigned to a_{1u}→e_{gy}-type transitions, while 317→320 and 318→321 are assigned to a_{1u}→e_{gx}-type transitions. Therefore, these calculated transitions at 638 and 607 nm can be assigned to the experimental Q bands at 694 nm, while those calculated at 590 nm can be associated to the observed band at 677 nm, respectively. The oppositely-signed MCD signals (692 and 672 nm) also support this assignment, since perpendicularly-polarized transitions give MCD signals of opposite sign [11, 12]. The band calculated at 588 nm also corresponds to a_{1u}→e_{gy}-type transitions. But this band is considerably weaker than the calculated 590 nm band so that the corresponding band cannot be found in the experimental spectrum. By using ZINDO/S Hamiltonian, the Q_Y and Q_X-polarized transitions of comparative intensity were calculated at 734 and 700 nm (Fig. 28, right).

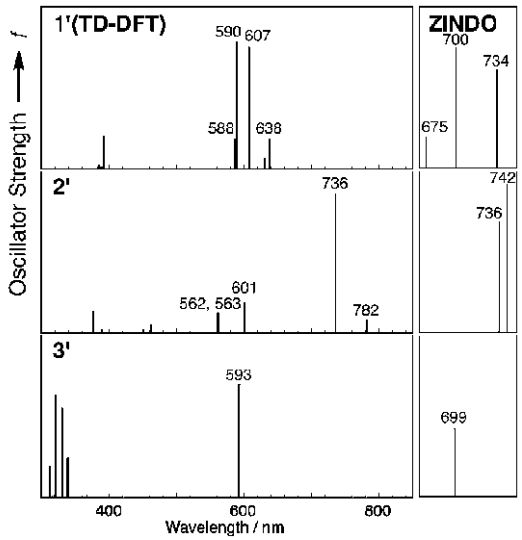

Fig. 28. Calculated absorption spectra of **1'** (top), **2'** (middle) and **3'** (bottom). Calculated at B3LYP/6–31G*, SVP for Zn (left) or ZINDO/S (right)

Рис. 28. Рассчитаные спектры поглощения **1'**(вверху), **2'** (посередине) и **3'**(внизу). Рассчитано методом B3LYP / 6–31G *, SVP для Zn (слева) или ZINDO/ S (справа)

The band calculated at 675 nm corresponds to z-polarized transitions, but its position cannot be assigned in the experimental spectrum since vibronic bands are considered to be superimposed in the same region. The analysis of **2** was conducted similarly. Based on the TD-DFT method at the B3LYP/631SVPs level, several mutually-perpendicularly polarized, and closely-lying allowed transitions were calculated at 782 and 736 nm in the near infrared region. These calculated transitions are assigned to the Q_y and Q_x bands, respectively, since these are also a_{1u}→e_g-type transitions ($^1E_u \leftarrow {}^1A_{1g}$ transition under D_{4h} symmetry). In the case of the ZINDO/S calculation, these bands were estimated at 742 and 736 nm as bands of comparative intensity (Fig. 28, right). The calculated small energy difference between the Q_x and Q_y bands supports the experimentally-observed single Q band of **2** (Fig. 27). From the data in Fig. 29, the small energy difference between the Q_x and Q_y bands may be attributable to the small energy difference between the LUMO and LUMO+1 of this molecule. Thus, this feature is close to those of metalloPcs of D_{4h} symmetry. Other allowed transitions were calculated at 601, 563, and 562 nm. These may be associated with an absorption peak at 709 nm and a MCD peak at 703 nm. The longer wavelength shift of the Q band of **2** compared to that of monomeric **3** can be ascribed to the smaller energy difference between the HOMO and LUMO in **2**.

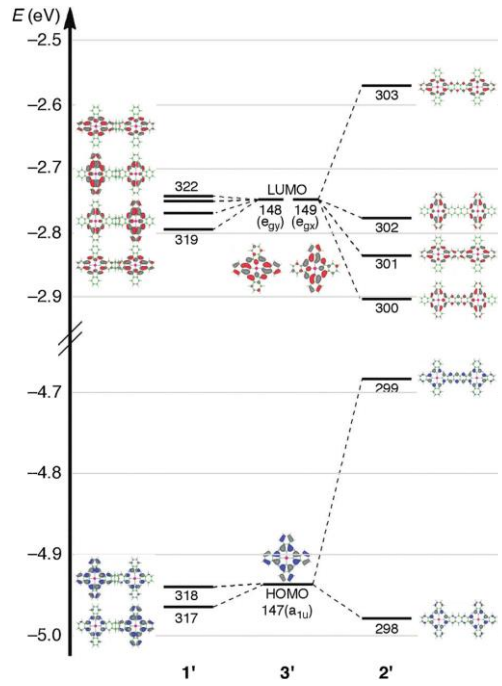

Fig. 29. Partial molecular energy diagram/orbitals of **1'**, **2'** and **3'**
Рис. 29. Диаграмма парциальной молекулярной энергии/орбитали **1'**, **2'** и **3'**

In order to further strengthen the above assignments, we have attempted simultaneous band deconvolution analyses for the experimental electronic absorption and MCD spectra (not shown). Band deconvolution analysis is carried out using the same number of components, same or very close energy, and same bandwidth for the absorption and MCD spectra, by fitting each band with a Gaussian line shape. The Q bands of both **1** and **2** were fitted with two Gaussian lines whose relative intensities are close to those estimated by calculation (*f* values in Table 3). In particular, the single Q band of **2** can be decomposed by two closely-lying (8 nm difference) components, supporting the reliability of the calculated data. Several types of conjugated, planar bis-Pcs sharing one benzene unit [37, 38, 41] or two benzene units (naphthalene unit) [39] have been reported to date. Our bis-ZnPc (**2**) shares three benzene units (anthracene unit) between the Pcs, where the only structural difference is the number of common benzene units. MO calculations on the basis of the PPP approximation of conjugated, planar bis-Pcs connected by different numbers of benzene rings have been attempted previously [37]. According to these reports, it is anticipated that the larger the distance between the two Pc centers, the smaller will be the splitting of the Q band. In accordance with this prediction, in the case of a conjugated, planar bis-Pc sharing one benzene ring, the splitting of the Q band is about 100 nm [37] and the MCD spectrum shows coupled pairs due to opposite Faraday B terms, while in the present **2**, it is considered that the splitting is so small (8 nm) that the Q band is observed as a single band. This in turn indicates that the interaction between the two Pc units can be explained by exciton type coupling. Thus, the conjugation between the two ZnPc units in **2** appears smaller than for a bis-Pc sharing a benzene unit [37, 38, 41].

Table 3

Partial molecular energy diagram/orbitals of 1', 2' and 3'. The calculated excitation wavelength (λ), oscillator strength (*f*) for the components of B3LYP/631SVPs (a) or the Q bands of 1', 2' and 3' calculated by ZINDO/S Hamiltonian (b)

Таблица 3. **Диаграмма парциальной молекулярной энергии/орбиталей 1', 2' и 3'. Рассчитанная длина волны возбуждения (λ), сила осциллятора (*f*) для компонентов B3LYP / 631SVPs (a) или Q-полос 1', 2' и 3', рассчитанные по гамильтониану ZINDO / S (b)**

Compd	l /nm	f	Composition (%)
(a)			
1^0	638	0.19	318 - 319 (84%)
	607	0.76	317 - 322 (83%), 318 - 319 (9%)
	590	0.78	317 - 320 (49%), 318 - 321 (45%)
	588	0.18	317 - 319 (39%), 318 - 322 (54%)
2^0	782	0.16	299 - 300 (97%)
	736	1.73	299 - 301 (99%)
	601	0.38	298 - 302 (91%), 299 - 304 (6%)
	563	0.15	299 - 304 (90%), 298 - 302 (5%)
	562	0.25	298 - 303 (96%)
3^0	593	0.42	147 - 148 (77%), 147 - 149 (17%)
	593	0.42	147 - 149 (77%), 147 - 148 (17%)
(b)			
1^0	734	1.53	195 - 196 (54%), 194 - 197 (43%)
	700	1.87	195 - 199 (48%), 194 - 198 (46%)
	675	0.48	195 - 197 (48%), 194 - 196 (46%)
2^0	742	2.28	189 - 190 (65%), 188 - 193 (31%)
	736	1.71	189 - 191 (56%), 188 - 192 (38%)
3^0	699	1.06	93 - 94 (93%)
	699	1.06	93 - 95 (93%)

As shown above, we have prepared two types of bis-ZnPc, and conducted their spectroscopic analyses in terms of electronic absorption and MCD spectroscopy. The spectroscopic properties of both gable-type **1** and the planar **2** containing a shared anthracene ring have been reasonably explained through the concept of exciton coupling. The unsplit Q band of **2** appears to be the result of weak exciton coupling between the constituting ZnPc units. This is, however, an unexpected result, considering that bis-ZnPc **2** is a molecule with D_{2h} symmetry and that the ratio between the long- and short axes is clearly fairly different.

b) Spectroscopic and Theoretical Studies of Optically Active Porphyrin Dimers: A System Uninterpretable by Exciton Coupling Theory [45]

In the case of chiral organic molecules containing two or more chromophoric units, the exciton- coupled CD method has been widely utilized as a versatile and sensitive method for determining their absolute

configurations and conformations [46]. One can assign the sense of chiral arrangement of the relevant chromophores from the sign of derivative-shaped CD signals generated by excitonic interactions between the transition electric dipole moments of two chromophores in a chiral environment. Although the exciton-coupled CD method has succeeded in determining the helical structures of many organic molecules, the application of this method is limited for independent chromophoric systems from a theoretical point of view [46]; the application of exciton coupling models requires spatially separated chromophoric units. Therefore, chiral systems such as helicenes are not suitable for application of this method. In addition, even if the system is regarded as an independent chromophoric system, the exciton chirality method could be misleading in the case of molecules such as biflavone, whose CD bands consist of many overlapping electronic transitions in a narrow energy region [47].

Recently, TDDFT has been developed for calculating the CD spectra of numerous chiral systems, including molecules unsuitable for the exciton chirality method [48-50]. Here we report the assignment of the helical sense of a chiral fused bis-porphyrin, namely, *meso-meso* β-β doubly linked bis-porphyrin **1** (Fig. 30a), based on a detailed analysis of the CD spectra and TDDFT calculations. The bis-porphyrin exhibits a significantly perturbed electronic absorption spectrum that indicates that remarkable π-conjugation exists in the system [51]. This implies that the two porphyrin systems cannot be considered as independent chromophores in the fused system.

According to the X-ray crystal structure [51], the two porphyrin rings adopt an almost coplanar, helically twisted conformation due to steric repulsion of the hydrogen atoms at the nearest pyrrole β position (Fig. 30b). The helical structure of the dimer was further confirmed by separation into two enantiomers on a chiral HPLC column. The optically active dimer thus obtained exhibited intense CD signals in the 300–800 nm region, but this system was discussed using exciton coupling theory [51].

To gain a better understanding of the electronic excited states, we also recorded MCD spectra of this compound, since CD and MCD analyses are mutually complementary in aiding the interpretation of excited states.

Fig. 31 shows the electronic absorption, CD and MCD spectra of an enantiomer of the doubly linked bis-porphyrin, which corresponds to the second eluting isomer obtained by chiral HPLC. The helical sense of the enantiomer is assigned as left-handed on the basis of the exciton chirality method in the previous paper [51]. As we have already reported, the absorption spectrum of the fused dimer contains significantly perturbed absorption bands compared to nickel tetraphenylporphyrin; intensely red shifted absorption bands were observed at 736 nm with a shoulder at about 820 nm.

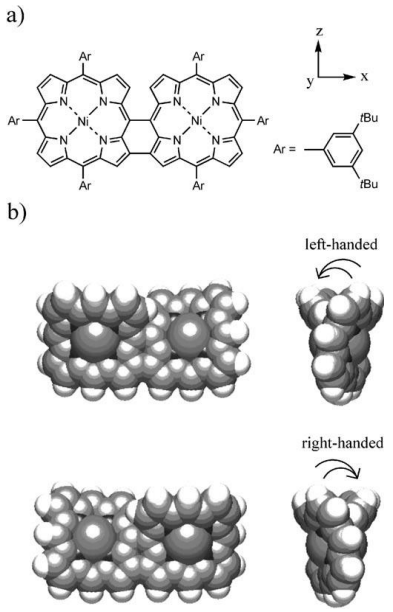

Fig. 30. a) Doubly linked bis-porphyrin **1**. b) Origin of chirality based on the crystal structure

Рис. 30. a) Двусвязный бис-порфирин **1**. b) Происхождение хиральности на основе кристаллической структуры

The enantiomer exhibited intense CD signals in the UV/Vis/ NIR region. The peak position of the CD signal of the lowest energy band was at 726 nm, blue-shifted by 10 nm from the absorption band. This should arise from the fact that there is a weak, negative CD signal corresponding to the absorption shoulder at about 820 nm. As expected, the CD spectrum of the first-eluting enantiomer is the mirror image of that of the second-eluting enantiomer of **1**.

The MCD intensities of the dimer were significantly weaker than those observed in typical porphyrin monomers, similar to other types of fused porphyrins [30, 37-39]. Thus, the MCD intensity $[\theta]_M$ of the present dimer is approximately 10 times weaker than that for the Soret band of nickel tetraphenylporphyrin. Since the MCD pattern associated with the absorption bands in the 650-850 nm region is essentially similar in shape to the corresponding absorption bands, these bands can be assigned to Faraday B terms. In addition, these MCD signs are positive, the reverse of typical porphyrin monomers. Note that an intense MCD signal was observed at 634 nm where there are no intense absorption and CD bands. This is because the selection rules of MCD spectra are different from those of electronic absorption spectra, since the MCD intensity

mechanism depends strongly on the magnetic dipole moment. In the case of D_{4h} porphyrins, relatively intense MCD signals are generally observed for the Q band, which has optically forbidden nature. Since mutually perpendicularly polarized transitions generally have differently signed MCD signals [11, 12, 19], the polarization of the 634 nm transition must be different from that of the 736 and 820 nm transitions. The MCD pattern in the higher energy region appears to be more complex, indicative of the many overlapping transitions with different polarizations.

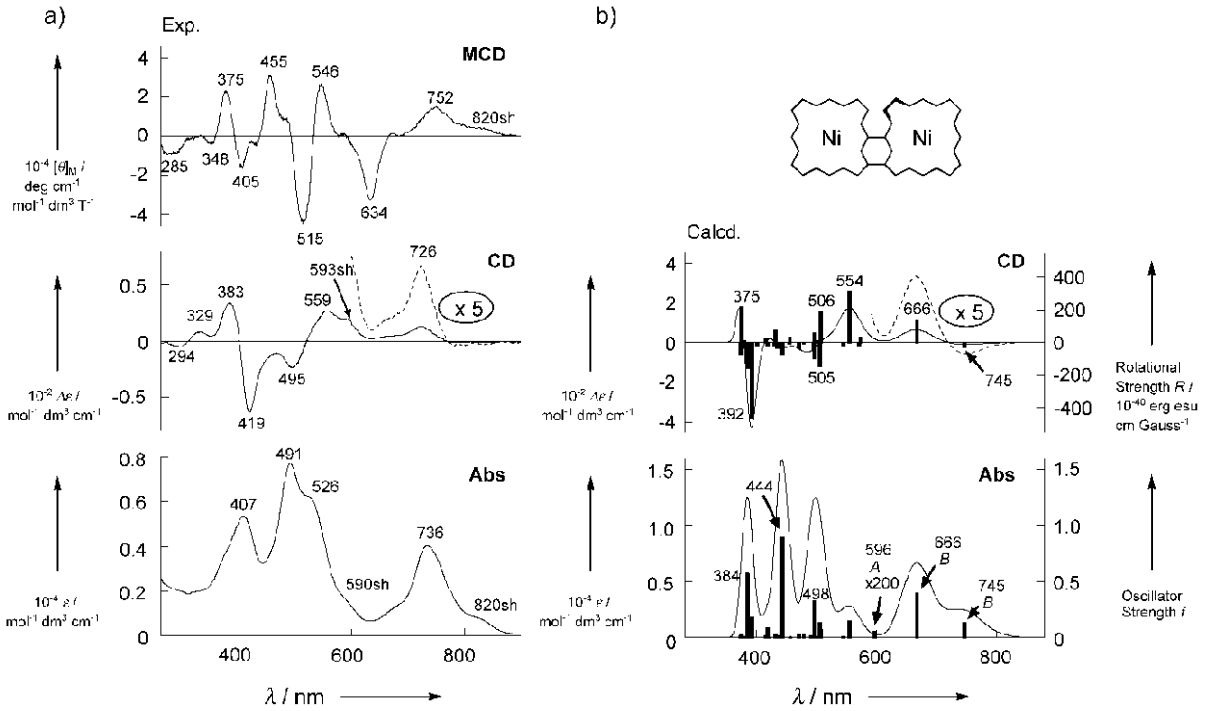

Fig. 31. a) Experimental MCD, CD, and electronic absorption spectra of the second-eluting enantiomer of **1**, in $CHCl_3$ at room temperature. b) Calculated CD and absorption spectra obtained as sums of a Gaussian-type function with a half-band width of 1300 cm^{-1} (left scale). The CD and absorption intensities are given in rotational strength ***R*** and oscillator strength ***f***, respectively (right scale). The absorption intensity at 596 nm is magnified 200 times. *A* and *B* are symmetry labels

Рис. 31. a) Экспериментальные спектры МКД, CD и электронного поглощения второго элюирующего энантиомера **1** в $CHCl_3$ при комнатной температуре. b) Рассчитанные CD и спектры поглощения, полученные в виде сумм функции гауссовского типа с шириной полуполосы 1300 $см^{-1}$ (левая шкала). Интенсивность CD и абсорбции даны в силе вращения ***R*** и силе осциллятора ***f*** соответственно (правая шкала). Интенсивность поглощения при 596 нм увеличивается в 200 раз. *A* и *B* - метки симметрии

To rationalize the relationship between the spectral features and helical structure of the fused bis-porphyrin, we performed geometry optimization calculations on a right-handed helical bis-porphyrin with C_2 symmetry at the DFT level of theory. Although not shown, the optimized geometry appears to be in agreement with the crystal structure (a significantly ruffled conformation) except for the peripheral phenyl groups. Forty excitation energies, oscillator strengths, and rotatory strengths were then calculated by using TDDFT to obtain theoretical electronic absorption and CD spectra. The calculated curves are obtained as sums of a Gaussian-type function with a half-band width of 1300 cm^{-1}. As is clearly seen in Fig. 31, both the theoretical absorption and CD spectral patterns reproduce the experimental spectral features remarkably well, although the calculations overestimate the excitation energy and intensity to some degree. Due to the C_2 symmetry, the transition from the ground state to an excited state with *A* symmetry corresponds to the z-axis polarized transition, while the transition to an excited state with *B* symmetry is polarized perpendicularly to the z axis. Many weak transitions with different polarization were predicted in the higher energy region, which are probably related to the observed complex MCD pattern.

The calculations predict two absorption bands at 666 and 745 nm, which are attributable, respectively, to the absorption bands observed at 735 nm and a shoulder observed at ca. 820 nm, judging from the positive and negative CD signs. Details of the assignments in this region are discussed below. As a consequence, we conclude that the helical sense of the optically active fused bis-porphyrin can be assigned to the right-handed helical geometry shown in Fig. 30. The present

assignment is opposite to the assignment reported previously on the basis of the exciton chirality method [51].

To comprehensively understand the electronic excited states of the *meso–meso* β-β doubly linked bis-porphyrin, a detailed MO analysis was carried out. Recently, we have shown that the frontier MOs of *meso–* β *meso–*β doubly linked bis-porphyrins and *meso–meso* β-β β-β triply linked oligoporphyrins consist of linear combinations of the constituent monomeric MOs, and that the effect of lowering the symmetry is always larger on the LUMO than on the HOMO [52]. The MO features were correlated with the observed MCD pattern of the Q transitions by applying Michl's perimeter model [11, 12]. Fig. 32 shows the frontier MOs of the chiral bis-porphyrin and nickel tetraphenylporphyrin. The frontier MOs of the bis-porphyrin are delocalized over the two porphyrin units, and consist of linear combinations of the constituent monomer MOs. The delocalized electronic system is enlarged by connecting the two porphyrin rings, which decreases the HOMO-LUMO gap. The stabilization energy of the LUMO is larger than the destabilization energy of the HOMO. These MO features are similar to those of other fused porphyrins [52]. Since the three lowest transitions obtained from the TDDFT calculations arise from these frontier MOs, the lowest three transitions of the bis-porphyrin can be assigned to the Q transitions. The two lowest transitions are optically allowed and arise from mixing of HOMO→LUMO and HOMO-1→LUMO transitions. The polarization of these transitions is perpendicular to the z axis. On the other hand, the third transition has an optically forbidden nature, arising from the mixing of HOMO-2→LUMO and HOMO→LUMO+2. The transition is polarized along the z axis. Since the MCD signals for two transitions with perpendicular polarizations give oppositely signed Faraday B terms [11, 12, 19], the positive MCD signal observed at 752 nm and the negative MCD signal observed at 634 nm can be assigned to the second and third Q transitions. The shoulder at about 820 nm is therefore assigned to the lowest energy Q transition. The positive/negative MCD sign sequence, in ascending energy, is related to destabilization of the LUMO [11, 12].

This work has demonstrated definitive band assignments of an optically active fused bis-porphyrin by inspection of the complete UV/Vis part of the observed spectroscopic properties in conjunction with TDDFT calculations. According to the coupled Faraday B terms observed in the 600-850 nm region, we unambiguously assigned short- and long-axis polarized Q transitions. As a result, we reassigned the helical conformation of the dimer. The assignment was opposite to the previous assignment based on the exciton chirality method. These results should have implications in the field of absolute stereochemistry: the point-dipole approximation is much too simple to describe the electronic excited states of conjugated porphyrins whose absorption spectra are significantly different from those of the constituent units.

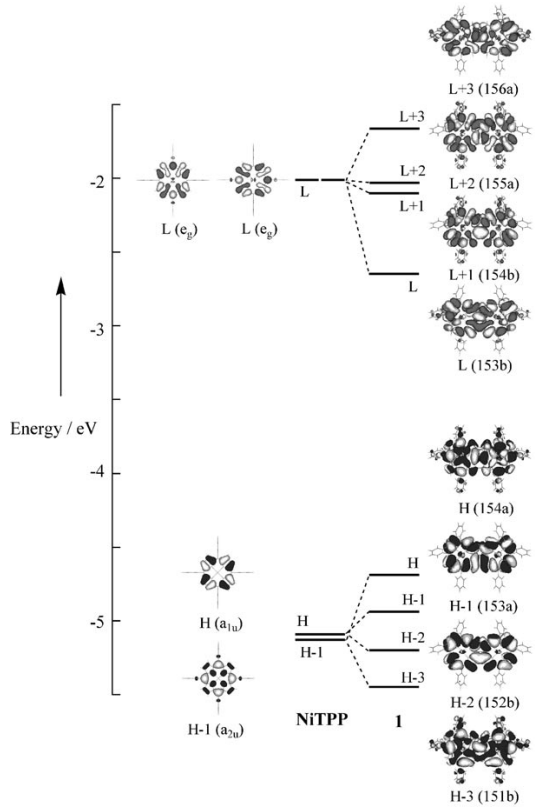

Fig. 32. Frontier MOs and energy levels of a *meso-meso* β-β linked bis-porphyrin and nickel tetraphenylporphyrin

Рис. 32. Граничные МО и энергетические уровни *мезо-мезо*-β- β связанного бис-порфирина и тетрафенилпорфирина никеля

TETRAMERIC SYSTEMS

Cofacial Type

A Discrete Quadruple-Decker Phthalocyanine [53]

The ability to form stacked sandwich-type phthalocyanine (Pc) oligomers in the presence of ions of metals such as lanthanides (Ln), yttrium, indium, and bismuth results in the formation of double- or triple-decker Pc complexes having unusual spectroscopic, electrochemical, and magnetic properties due to their π systems and/or f electrons [54]. No larger discrete stacked oligomer congeners have been reported to date, however, although mixtures of higher-order oligomeric species have been detected by mass spectrometry for mercury [55] and cadmium [56] complexes. Since the Pc ligand is a dianion [Pc(2-)] and

lanthanide ions are present as trivalent cations (Ln^{III}), $LnPc_2$ formation results in an anionic species (the blue form) unless the complex is oxidized to form a neutral $[LnPc_2]^0$ radical (the green form). In this sense, Ln_2Pc_3 can be regarded as the $[LuPc_2]^-$ blue form coordinated by an $[Ln^{III}Pc(2-)]^+$ species. It is clear on this basis that $[LuPc_2]^-$ can potentially stack a second $[LuPc_2]^-$ species through coordination with an appropriate central metal ion. Accordingly, we report the preparation of **1**, the first example of a discrete quadruple-decker Pc [53, 57]. The Cd^{2+} ion was selected to form a neutral complex with two stacked $[LuPc_2]^-$ units. Cook and co-workers have recently reported that Cd^{2+} has the ability to form sandwich-type Pc complexes [56]. A mixture of an unsubstituted $[LuPc_2]^-[NBu_4]^+$ species [58] and cadmium acetate $[Cd(OAc)_2 \cdot 2H_2O]$ was heated at 400 °C for 30 min under argon. Chromatographic separation of the resulting mixture gave **1** as a dark-purple powder in 3.4% yield (Scheme 6).

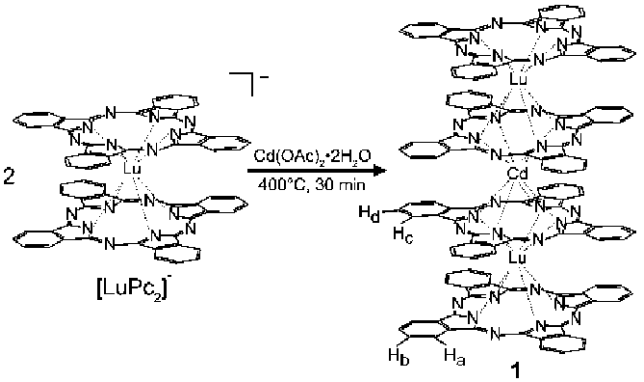

Scheme 6. Synthesis of **1**
Схема 6. Синтез соединения **1**

A molecular-ion peak was observed at *m*/*z* 2512.3883 (calcd for **1**: *m*/*z* 2512.3873) in a ESI-FTICR mass measurement. Elemental analysis results were consistent with a neutral structure having no counterions (C 61.59, H 2.99, N 17.41; calcd for $C_{128}H_{64}N_{32}Lu_2Cd$, C 61.19, H 2.57, N 17.84). The complex was stable in air at ambient temperatures in the solid state and moderately stable in solution for a couple of days. However, the complex tended to decompose to double-decker Pcs when CH_2Cl_2 or $CHCl_3$ solutions were allowed to stand for more than 1 week, making the growth of single crystals for X-ray crystallography problematic.

A quadruple-decker structure contains distinct sets of outer and inner Pc ligands. The ^1H NMR spectrum of **1** (not shown) exhibits three sets of proton signals at 8.59, 8.43, and 7.87 ppm with an integration ratio of 2:1:1, respectively, indicating the presence of two nonequivalent types of Pc ligands. The ^1H-^1H COSY spectrum demonstrated that the latter two sets of protons are correlated with each other, while the signal at 8.59 ppm exhibits no correlation with any other protons. Since it is known that the ^1H signals of the inner Pc of triple-decker complexes lie at higher frequencies than those of the two outer Pc rings and that the signals of α protons typically appear at higher frequencies than those of β protons, the signals at 8.43 and 7.87 ppm can be assigned to the H_α and H_β protons of the outer Pcs, while the signal at 8.59 ppm can be assigned to the inner Pcs [56]. The nuclear Overhauser effect (NOE) experiment demonstrated that irradiation of the signal at 8.59 ppm induces NOEs in the other two signals, since the two nonequivalent Pcs lie in close proximity. There are seven distinct carbon signals at 160.62, 156.48, 137.33, 130.66, 129.33, 124.55, and 122.44 ppm in the ^{13}C NMR spectrum. The eighth signal, which would be anticipated for a discrete quadruple-decker structure, is probably obscured by the solvent peaks. The results of the ^{13}C -^1H COSY and DEPT90 experiments were also found to be broadly consistent with this structure type.

Fig. 33 contains the absorption (bottom) and MCD (top) spectra of **1** in $CHCl_3$. Three distinct absorption bands at 332, 623, and 727 nm were observed. The latter two peaks are shifted to longer wavelength relative to the spectrum of $[LuPc_2]^-$ [27]. Since the derivative-shaped signals observed in the MCD spectrum closely resemble the Faraday *A* terms observed for complexes with a threefold or higher axis of symmetry, the main π-π* excited states either retain the orbital degeneracy of the corresponding Pc monomer states or have only relatively minor zero-field splittings. The spectra of **1** closely resemble those of the $[LuPc_2]^-$ blue form and Lu_2Pc_3 rather than those of the $[LnPc_2]^0$ green form, and all four Pc ligands can therefore be assigned a formal charge of 2-. The intensity ratio of the major bands in the 500-800 nm region is reduced from the value of 0.48 observed for $[LuPc_2]^-$ in $CHCl_3$ to 0.24. According to a theoretical approach developed by Ishikawa and co-workers [59], the spectral changes caused by the stacking of Pc monomers can be interpreted on the basis of exciton (EC) states generated by the excitation of a single ligand and charge resonance (CR) states generated by charge transfer between Pc rings. A lower-energy band with lower intensity typically arises from a transition with more CR character, while a more intense band at slightly higher energy arises primarily from an EC interaction. Since the electronic structure of **1** is broadly similar to that of $[LuPc_2]^-$, the bands observed at 623 and 727 nm can be assigned as Q bands arising from EC- and CR-dominated transitions, respectively.

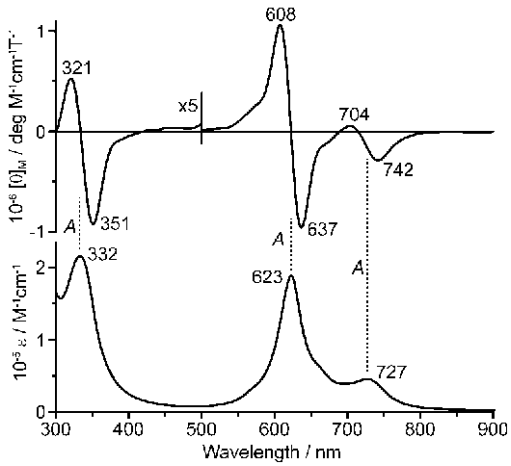

Fig. 33. (bottom) Absorption and (top) MCD spectra of **1** in $CHCl_3$

Рис. 33. (внизу) Спектры поглощения и (вверху) МКД **1** в $CHCl_3$

The quadruple-decker structure of **1** undergoes four reversible one-electron oxidation steps ($E_{1/2}$ = -0.26, 0.05, 0.46, and 0.77 V vs Fc^+/Fc) and four reversible one-electron reduction steps ($E_{1/2}$ = -1.16, -1.49, -1.81, and -2.05 V), while the corresponding cyclic voltammograms of $[LuPc2]^-$ contain two oxidation and up to three reduction couples under the same conditions. The gap between the first reduction and oxidation potentials is narrower in the case of **1**. This "stacking effect" has been reported previously for lutetium naphthalocyanine triple-decker and μ-oxo silicon Pc oligomers [60].

The potential barrier for oxidation/reduction steps is decreased because the positively charged hole in the HOMO or electron in the LUMO introduced by the redox process is delocalized over all four Pc rings. In summary, we have succeeded in synthesizing the first example of a discrete quadruple-decker Pc tetramer, **1**, through the reaction of $[LuPc_2]^-$ with cadmium acetate. The structure of **1** has been unambiguously established by high-resolution mass spectrometry, elemental analysis, and NMR spectroscopy. As anticipated, the optical spectra of **1** are broadly similar to those of $[LuPc_2]^-$. However, significant bathochromic shifts and a change in the intensity ratio of the EC- and CR-related Q bands are observed as a result of the formation of a multilayered oligomeric π structure. The electrochemical data also provide evidence for the stacking effects that would be anticipated for a quadruple-decker Pc complex.

Planar Type

A Directly Fused Tetrameric Porphyrin Sheet and Its Anomalous Electronic Properties That Arise from the Planar Cyclooctatetraene Core [61]

We report herein the synthesis and characterizations of a square-planar porphyrin sheet **3**, which is, to the best of our knowledge, the first example of two-dimensionally π-extended porphyrinic systems caused by symmetric direct fusion of four porphyrins. The molecule **3** is of great interest, because it allows for direct comparison of molecular morphology effects, linear versus square, upon the overall electronic properties of fused-conjugation of porphyrins. The electronic network of **3** consists of only porphyrins and thus is also interesting from a viewpoint of its analogy with those of polyacene and graphene analogues. Anomalous electronic properties of **3** that differ significantly from those of usual porphyrins particularly in respect of aromaticity will be discussed in relation to the structural motif of its enforced planar cyclooctatetraene (COT) core.

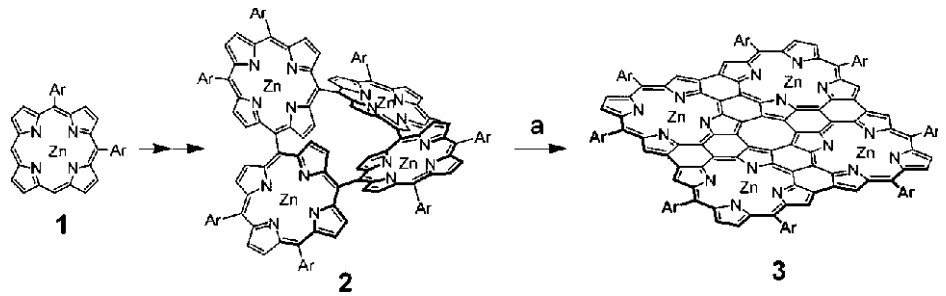

Scheme 7. Synthesis of **3**

Схема 7. Синтез соединения **3**

As a starting substrate, we employed directly *meso-meso* linked cyclic porphyrin tetramer **2** that was prepared from **1** through a stepwise coupling reaction sequence [62]. In toluene, **2** was treated with 30 equiv of DDQ and $Sc(OTf)_3$ at 55 °C for 5 h followed by separation over a short alumina column to provide **3** as black solids in 77% yield (Scheme 7). Inherent poor solubility of **3** can be improved by addition of a small amount of butylamine, which was quite important for its separation, final purification, and ^1H NMR measurements. MALDI-TOF-MS revealed the parent ion peak of **3** at *m/z* = 2977.4 $[M^+]$ (calcd for $[C_{192}H_{184}N_{16}Zn_4]^+$ = 2977.2). In accord with the highly symmetric structure, the ^1H NMR spectrum of **3** in

$CDCl_3$ containing 1% butylamine exhibited two singlets at 5.98 and 6.14 ppm for the porphyrin β-protons and a doublet at 7.01 ppm and a triplet at 7.29 ppm for the *ortho*- and *para*-protons of the *meso*-aryl substituents, respectively (Fig. 34).

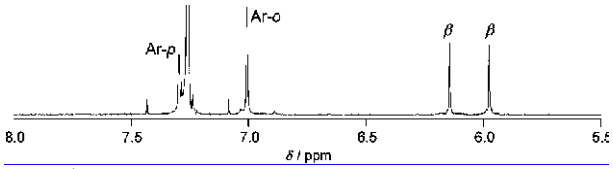

Fig. 34. ^{1}H NMR spectrum of **3** in $CDCl_3$ containing 1% butylamine
Рис. 34. ^{1}H ЯМР-спектр **3** в $CDCl_3$, содержащем 1% бутиламина

The porphyrin sheet **3** exhibits considerably broadened absorption bands in the wide range from UV-visible to near- IR (Fig. 35a, bottom), which can be roughly divided into three distinct spectral regions, Band **I** (300-600 nm), Band **II** (600-1000 nm), and Band **III** (1000-1500 nm). Band **III** is considerably weaker as compared to that of one-dimensional tetrameric porphyrin tape. The MCD spectrum of **3** shows weak and intense signals for Bands **I** and **II**, respectively (Fig. 35a, top). Because these spectral features have first derivative shapes, these signals can be assigned as Faraday *A* terms arising from transitions from a nondegenerate level to a degenerate level [11, 12].

Notably, a distinct negative Faraday A term is observed for Band **II**, that is, positive/negative signs in ascending energy as a rare case, which is in contrast to positive Faraday A terms that are usually observed for porphyrin skeletons. The MCD spectral pattern for the Band **III** region has been assigned as Faraday B terms, because the spectrum is similar to those of the absorption spectra, which indicates that the bands can be assigned as transitions between nondegenerate states. The absorption spectrum has been simulated using time-dependent Hartree-Fock theory based on the ZINDO/S Hamiltonian (TDHF-ZINDO/S) on *meso*-phenyl-substituted porphyrin sheet **3**$_{Ph}$ as shown in Fig. 35b. Two intense absorption bands are predicted at 479 nm (oscillator strength f = 2.930) and 640 nm (f = 2.377), which can be assigned as the main electronic transitions of Bands **I** and **II**, respectively. The predicted excited states (E_u) are doubly degenerate, which leads to a prediction of Faraday *A* terms in the MCD spectrum. Two dipole-forbidden transitions (1177 nm (A_{2g}), f = 0 and 1056 nm (B_{1g}), f = 0) and an allowed transition with weak oscillator strength (965 nm (E_u), f = 0.016) are predicted in the Band **III** region. The broad and weak Faraday B terms observed for Band **III** can be associated with these three transitions, because absorption intensity could arise either from vibronic couplings or from a reduction of the ideal D_{4h} symmetry.

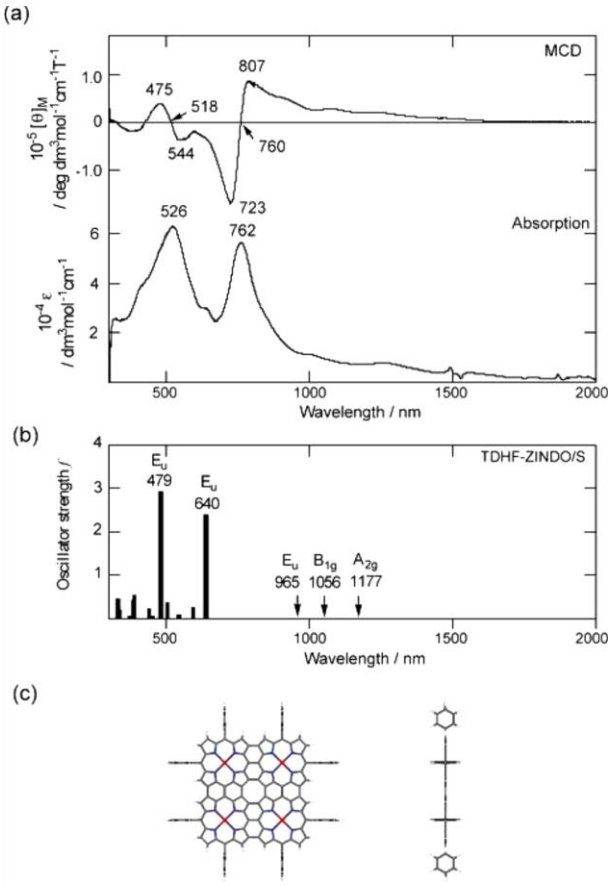

Fig. 35. (a)Experimental MCD (top) and absorption (bottom) spectra of **3** recorded in pyridine-d_5 at room temperature. (b) Stick absorption spectrum of **3**$_{Ph}$ calculated by TDHF-ZINDO/S method. (c) Calculated structure of **3**$_{Ph}$; top view (left) and side view (right)
Рис. 35. а) Экспериментальные спектры МКД (вверху) и поглощения (внизу) **3**, записанные в пиридине-d_5 при комнатной температуре. (b) Спектр поглощения **3Ph**, рассчитанный методом TDHF-ZINDO / S. (c) Расчитанная структура **3**$_{Ph}$; вид сверху (слева) и вид сбоку (справа)

The origin of the unusual spectral features can be readily deduced from the orbital degeneracies of the frontier molecular orbitals (MOs) of the π-system (Fig. 36). In the case of metalloporphyrins, the LUMO is typically orbitally degenerate (e_g) and the HOMOs are typically accidentally near degenerate (a_{1u} and a_{2u}) [7]. In contrast, both the HOMO (328, a_{1u}) and the LUMO (329, b_{1u}) of **3**$_{Ph}$ are nondegenerate. The low-energy Faraday B terms in the Band **III** region can be readily accounted for on this basis. The calculated 640 nm band is predicted to arise from a transition linking a degenerate orbital with a nondegenerate one (such as 322(323)→329 and 325(326)→330), whereas the 479 nm band is predicted to arise primarily from a transition linking a nondegenerate orbital and a degenerate one (i.e., electron-dominating transition). Negative Faraday A terms tend to arise from transitions in which orbital angular momentum (OAM) is greater in the ground state than in the excited state, while positive

Faraday A terms are associated with transitions where OAM is greater in the excited state. Because the OAM associated with electron circulation would normally be anticipated to be greater within a degenerate orbital, the results obtained from the TDHF-ZINDO/S calculation are consistent with the positive and negative Faraday A terms observed for Bands **I** and **II**, respectively.

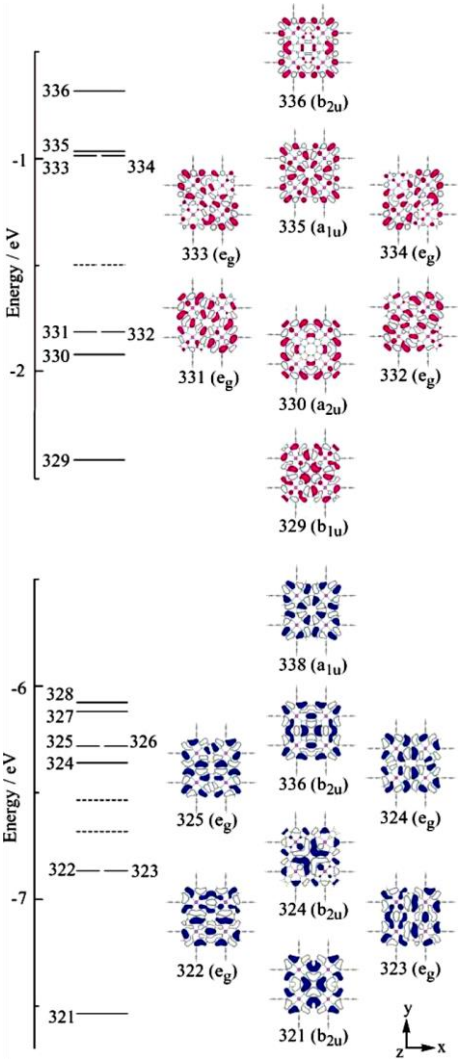

Fig. 36. Frontier molecular orbital diagram and contour plots of occupied and virtual orbitals of **3**$_{Ph}$ (TDHF-ZINDO/S). The dotted lines indicate four frontier molecular orbitals of D_{4h} zinc tetraphenylporphyrin (Zn-TPP)

Рис. 36. Диаграмма границы молекулярной орбитали и контурные графики занятых и виртуальных орбиталей **3**$_{Ph}$ (TDHF-ZINDO / S). Пунктирные линии показывают четыре пограничные молекулярные орбитали D_{4h}-тетрафенилпорфирина цинка (Zn-TPP)

CONCLUSIONS

In the monomeric systems [57, 63], we first reported the relationship between symmetry of porphyrinic π-conjugated systems and singlet oxygen yields (Φ_Δ). The Φ_Δ value generally decreased in the order of Zn>Mg>H2, and it became evident that the S_1-T_1 ISC is the most important process in the relationship between the molecular symmetry and Φ_Δ value. In one azulene-fused porphyrin, the ΔHOMO was very similar to ΔLUMO in both MCD spectra and MO calculations, while two-azulene-fused porphyrins showed an MCD spectrum characteristic of ΔHOMO < ΔLUMO, which was supported by MO calculations. Four azulene-fused porphyrin, on the other hand, showed a spectrum indicating ΔHOMO > ΔLUMO. In the case of an N-confused porphyrin, data were analyzed based on the relative size of ΔHOMO and ΔLUMO. The effective chromophore symmetry was controlled by linking four electron-withdrawing and four electron-releasing groups at desired β-positions of four pyrrole rings. The D_{2h} type arrangement of these groups yielded the compound having the largest Q-band splitting. Phosphorus(V) was inserted into the center of tetraazaporphyrins, and these compounds showed a strong CT band between the Q and Soret bands, due to the highly positive P(V) ion. In the case of Cu-corrole and Cu-benzocorrole, we showed that the interaction between the substrate surface changes, depending on whether the electron resides in the *d*-orbital of Cu or on the corrole ligand. We have also succeeded in deforming the Pc skeleton by introducing bulky substituent groups at the α-positions. With the increasing deformation, the Q band shifted to longer wavelength and the energy difference between the first oxidation and reduction potentials decreased, which is mainly due to the extraordinary destabilization of the HOMO.

In non-planar deformed systems, we reported that deformation strongly affects the spectroscopic and electrochemical properties. The effect was concretely estimated by comparing the data with those of planar systems. Azaphenalene-fused Pc derivatives exhibited a fairly deformed structure due to the six-membered units around the central core. The C_{2v}-type isomer showed an unsplit Q band, while the D_{2h}-type isomer showed a largely split Q band, in accord with the results from group theory. In the case of saddle-shaped ZnPc, we showed that protonation occurred at the *meso*-nitrogen due to the high basicity of the inner core. Although the pyrrole nitrogens of normal Pcs are surrounded by five-membered pyrrole rings, in azepiphthalocyanine containing one seven-membered ring, part of the Pc plane is severely distorted, so that it exhibited a significantly twisted structure and a large splitting of the Q-band absorption, indicative of its azachlorin-like π-conjugation system. Superazaporphyrin consisting of five pyrrole rings was obtained by uranium-templated cyclization of proline rings. It showed a Q band absorption at around 880 nm, which is much longer than that of azaporphyrin (ca. 640 nm).

Subporphyrin, consisting of three pyrrole rings, was reported for the first time as a ring-shrunk porphyrin. This compound was obtained by reacting tripyrrolylborane and benzaldehyde. It has a cone-shaped structure, and showed the Q and Soret bands at around 450-500 and 370-380 nm, respectively, reflecting the smaller π-conjugation structure compared to regular porphyrins. *meso*-Aryl-Substituted [14] Triphyrin(2.1.1) was also prepared, and its structure and spectroscopic properties compared with those of subporphyrins. Although triphyrin has one more *meso*-carbon than subporphyrins, it has a planar structure, and the Q band spreads over the region 450-600 nm.

Core-modified rubyrins containing dithienylethene moieties were the first reported ring-expanded systems. Due to the ring-closing and -opening ability of the dithienylethene moiety, the spectroscopic character changed between the 4*n*π (open form) and (4*n*+2)π systems (closed form). Rectangular-shaped expanded phthalocyanines with two central molybdenum or tungusten atoms were prepared, and their structures characterized using several spectroscopic techniques. Although six isomeric structures were first considered from the mass data, the possibility was reduced to two structures based on the X-ray crystallographic data, and finally by taking experimental absorption, calculated absorption and -IR into account, the structure was determined. These exhibited the Q band between 1500 and 800 nm, while the Soret band appeared at ca. 400-550 nm. Norcorroles of superphthalosyanines, i.e. pentabenzotriazasmaragdyrins, were prepared by bottom-up synthesis. A phthalonitrile dimer was first obtained by reacting a phthalonitrile in thiol in the presence of Na^+, and this dimer and other phthalonitrile units were heated at 200 °C. From the reaction mixture, the desired pentabenzotriazasmaragdyrins consisting of five isoindole units and three *meso*-nitrogens were isolated. These showed typical absorption spectra of 4*n*π aromatic systems.

As cyclo[n]pyrroles, we have prepared those of n = 6,8,10 with and without fused aromatic rings, and compared their spectroscopic properties. With fusion of aromatic ring and increase of n, the Q band shifted to longer wavelength and intensified. The negative Faraday A MCD terms were theoretically explained since ΔLUMO > ΔHOMO ~ 0 when n is an even number. When n = 10, the Q band appeared at ca. 2000 nm.

The introduction of a P(V) ion to octaphenylated tetraazaporphyrin produced a stable (4*n*+3)π type radical, which appeared to be realized due to the strongly electron-withdrawing P(V) ion.

As an example of cofacial type dimers, we reported the phthalocyanine (Pc)-O-naphthalocyanine μ-oxo Si dimer. This showed solvatochromic behavior, so that different spectra were obtained in $CHCl_3$ and toluene, which might be produced by rotation of the Pc and Nc units about the z-axis. The spectra of cofacial porphynato-naphthalocyaninato rare-earth dimeric and trimeric compounds were theoretically reasonably and definitively assigned by considering the relevant interactions of Gouterman's four orbitals of the constituent chromophores. The position, sign of MCD terms, and intensity were clearly explained, since all of the compounds had a similar rotation degree between porphyrin and naphthalocyanine moieties with respect to the z-axis. As optically-active mixed phthalocyaninato–porphyrinato rare-earth double-decker complexes, we have synthesized TPP-binaphthylated Pc Y and Eu complexes. These complexes showed interconvertible solvatochromic behavior in DMF and $CHCl_3$. Based on simulations using MO calculations, it was concluded that these molecules preferentially adopt a right-handed helical geometry (θ = 13°) with respect to the staggered conformation (θ = 0°) in DMF while θ = -2° in $CHCl_3$. Using tetracyano-paracyclophane, the Zn complex of *anti*-[2,2](1,4)phthalocyaninophane was prepared. This showed a split Q band, since the long-axis polarized transitions shifted to lower energy due to conjugation through the paracyclophane moiety. Similarly, as cyclophanes containing bowl-shaped aromatic chromophores, three isomers of *anti*-[2.2](1,4)subphthalocyaninophane were prepared using tetracyano-paracyclophane, tetrafluorophthalonitrile, and BCl_3 as a template. From the reaction mixture, the three isomers were separated by column chromatography. The sharp Q band of the concave-concave isomer broadened in the concave-convex isomer, and finally split into two peaks in convex-convex isomers, due to the practical increase of the long axis in this order.

A planar bis-phthalocyanine containing a shared anthracene unit was derived from zinc gable phthalocyanine. Compared with the previously-reported corresponding dimers sharing common benzene or naphthalene units, the splitting of the Q band decreased in this order, and this was supported by MO calculations. Although the Q band position was shifted significantly to longer wavelength (784 nm) compared with that of the constituting monomer (680 nm), the Q band splitting was not recognized in the anthracene-linked dimer. We also reported the assignment of the helical sense of a chiral fused bis-porphyrin, *meso-meso* β–β doubly linked bis-porphyrin, which was previously wrongly assigned based on exciton coupling theory. The absorption, CD, and MCD spectra were reasonably reproduced and assigned by MO calculations.

A cofacial tetrameric Pc was realized by linking two cofacial Lu Pc sandwich dimers by a Cd ion.

Its formation was confirmed by mass and NMR spectroscopy. The synthesis of a directly fused tetrameric porphyrin sheet and its anomalous electronic properties which arise from the planar cyclooctatetraene core were described. In this complex, the cyclooctatetraene core has a planar structure, although cyclooctatetraene generally has a cofacial structure. The Soret band splits into two strong peaks and a weak absorption tail spreads across the 1000-2000 nm region. Both the HOMO and LUMO were not degenerate, and a negative Faraday A MCD term corresponding to the Soret band at longer wavelength was rationalized by MO calculations.

Acknowledgement

This work was partly supported by Grant-in - Aid for Scientific Research (C), No. 18K05076, from the JSPS.

REFERENCES
ЛИТЕРАТУРА

1. **Oniwa K., Shimizu S., Shiina Y., Fukuda T., Kobayashi N.** A μ-oxo Hetero Dimer of Silicon Phthalocyanine and Naphthalocyanine. *Chem. Commun*. 2013. V. 49. P. 8341-8343.
2. **Ciliberto E., Doris K.A., Pietro W.J., Reisner G.M., Ellis D.E., Fragala I., Herbstein F.H., Ratner M.A., Marks T.J.** The π-π Interactions and Bandwidths in Molecular Metals. A Chemical, Structural, Photoelectron Spectroscopic, and Hartree-Fock-Slater Study of Monomeric and Cofacially Joined Dimeric Silicon Phthalocyanines. *J. Am. Chem. Soc.* 1984. V. 106. P. 7748-7761.
3. (a) **Kleinwachter J.** PhD thesis. Germany: University of Tubingen. 1994.; (b) **Li Z. Y., Lieberman M.** Axial Reactivity of Soluble Silicon(IV) Phthalocyanines. *Inorg. Chem.* 2001. V. 40. P. 932-939.
4. (a) **Ferencz A., Neher D., Schulze M., Wegner G., Viaene L., Deschryver F.C.** Synthesis and Spectroscopic Properties of Phthalocyanine Dimers in Solution. *Chem. Phys. Lett.* 1995. V. 245. P. 23-29; (b) **Oddos Marcel L., Madeore F., Bock A., Neher D., Ferencz A., Rengel H., Wagner G., Kryschi C., Trommsdorff H.P.** Electronic States and Relaxation Dynamics of Silicon Phthalocyanine Dimers. *J. Phys. Chem.* 1996. V. 100. P. 11850-11856.
5. **Kleinwachter J., Hanack M.** Rotational Isomers in Stacked Macrocycles: Synthesis and Spectroscopic Properties of Peripherally Substituted (μ-Oxo)bis(phthalocyaninatosilicon) Compounds. *J. Am. Chem. Soc.* 1997. V. 119. P. 10684-10695.
6. **Muranaka A., Matsumoto Y., Uchiyama M., Jiang J., BianY., Ceulemans A., Kobayashi N.** Definitive Assignments of the Visible−Near-IR Bands of Porphyrin-Naphthalocyanine Rare-Earth Sandwich Double- and Triple-Decker Compounds by Magnetic Circular Dichroism Spectroscopy. *Inorg. Chem.* 2005. V. 44. P. 3818-3826.
7. **Gouterman M.** In: The Porphyrins. Ed. by D. Dolphin. New York: Academic Press. 1978. V. 3. Chap. 1.
8. (a) **Ishikawa N., Kaizu Y.** Disappearance of MCD A Term in the Fingerprint Band of Cation Radicals of Phthalocyanine Metal Complexes. *Chem. Phys. Lett.* 2001. V. 339. P. 125-132. (b) **Ishikawa N., Ohno O., Kaizu Y.** Electronic States of Bis(phthalocyaninato)lutetium Radical and Its Related Compounds: The Application of Localized Orbital Basis Set to Open-Shell Phthalocyanine Dimers. *J. Phys. Chem.* 1993. V. 97. P. 1004-1010.
9. **Ricciardi G., Rosa A., Baerends E.J., van Gisbergen S.A.J.** Electronic Structure, Chemical Bond, and Optical Spectra of Metal Bis(porphyrin) Complexes: A DFT/TDDFT Study of the Bis(porphyrin) M(IV) (M=Zr, Ce, Th) Series. *J. Am. Chem. Soc.* 2002. V. 124. P. 12319-12334.
10. **Jiang J., Bian Y., Furuya F., Liu W., Choi M.T.M., Kobayashi N., Li H.-W., Yang Q., Mak T.C.W., Ng D.K.P.** Synthesis, Structure, Spectroscopic Properties, and Electrochemistry of Rare Earth Sandwich Compounds with Mixed 2,3-Naphthalocyaninato and Octaethylporphyrinato Ligands. *Chem. Eur. J.* 2001. V. 7. P. 5059-5069.
11. **Michl J.** Magnetic Circular Dichroism of Cyclic. Pi.-electron Systems. 1. Algebraic Solution of the Perimeter Model for the A and B Terms of High-Symmetry Systems with a (4N+2) π-Electron [n] Annulene Perimeter. *J. Am. Chem. Soc.* 1978. V. 100. P. 6801-6811.
12. **Michl J.** Magnetic Circular Dichroism of Cyclic. Pi.-electron Systems. 2. Algebraic Solution of the Perimeter Model for the B Terms of Systems with a (4N +2) π-Electron [n] Annulene Perimeter. *J. Am. Chem. Soc.* 1978. V. 100. P. 6812-6818.
13. **Michl J.** Electronic structure of aromatic π-electron systems as reflected in their MCD spectra. *Pure. Appl. Chem.* 1980. V. 52. P. 1549–1563.
14. **Michl J.** Magnetic Circular dichroism of Aromatic Molecules. *Tetrahedron* 1984. V. 40. P. 3845–3934.
15. **Zhang X., Muranaka A., Lv W., Zhang Y., Bian Y., Jiang J., Kobayashi N.** Optically Active Mixed Phthalocyaninato–Porphyrinato Rare-Earth Double-Decker Complexes: Synthesis, Spectroscopy, and Solvent-Dependent Molecular Conformations. *Chem. Eur. J.* 2008. V. 14. P. 4667–4674.
16. **Lu H., Kobayashi N.** Optically Active Porphyrin and Phthalocyanine Systems. *Chem. Rev.* 2016. V. 116. P. 6184-6261.
17. For example, the electronic absorption data for [YH{Pc(α-$OC_4H_9)_8$}(TClPP)] in DMF λ_{max} (log ε): 325 (5.05), 418 (5.49), 495 (4.83), 596 (4.50), 654 (4.70), 853 (4.51), 933 nm (4.33); in $CHCl_3$ λ_{max} (log ε): 323 (4.85), 418 (5.40), 498 (4.75), 571 (4.20), 627 (4.56), 880 (sh), 954 nm (4.20); the electronic absorption data for [Y(Pc)(TClPP)] in DMF λ_{max} (log ε): 335 (4.89), 391 (4.74), 412 (5.01), 479 (4.63), 586 (4.28), 637 (4.29), 814 nm (4.14); in $CHCl_3$ λ_{max} (log ε): 332 (4.92), 401 (5.03), 470 (4.70), 732 (3.55), 1034 (3.79), 1238 (3.91), 1656 nm (3.49); the data for [Y(Pc)(TClPP)] in $CHCl_3$ are cited from: **Lu F., Sun X., Li R., Liang D., Zhu P., Zhang X., Choi C.-F., Ng D. K. P., Fukuda T., Kobayashi N., Jiang J.** Synthesis, Spectroscopic Properties, and Electrochemistry of Heteroleptic Rare Earth Double-Decker Complexes with Phthalocyaninato and meso-Tetrakis(4-chlorophenyl)porphyrinato Ligands. *New J. Chem.* 2004. V. 28. P. 1116-1122.
18. **Ng D.K.P., Jiang J.** Sandwich-Type Heteroleptic Phthalocyaninato and Porphyrinato Metal Complexes. *Chem. Soc. Rev.* 1997. V. 26. P. 433–442.
19. **Mack J., Stillman M.J., Kobayashi N.** Application of MCD Spectroscopy to Porphyrinoids. *Coord. Chem. Review*. 2007. V. 251. P. 429-453.
20. **Kobayashi N., Nakai K.** Applications of Magnetic Circular Dichroism Spectroscopy to Porphyrins and Phthalocyanines. *Chem. Commun. (Feature Article).* 2007. P. 4077-4092.
21. **Mack J., Kobayashi N.** Low Symmetry Phthalocyanines and Their Analogues. *Chem. Rev.* 2011. V. 111. P. 281-321.
22. a) **Kobayashi N., Kobayashi Y., Osa T.** Optically Active Phthalocyanines and Their Circular Dichroism. *J. Am. Chem. Soc.* 1993. V. 115. P. 10994–10995; b) **Kobayashi N.** Opti-

cally Active 'Adjacent' Type Non-Centrosymmetrically Substituted Phthalocyanines. *Chem. Commun.* 1998. P. 487–488; c) **Kobayashi N., Higashi R., Titeca B. C., Lamote F., Ceulemans A.** Substituent Induced Circular Dichroism in Phthalocyanines. *J. Am. Chem. Soc.* 1999. V. 121. P. 12018–12028.

23. **Wang R., Li R., Li Y., Zhang X., Zhu P., Lo P.-C., Ng D.K.P., Pan N., Ma C., Kobayashi N., Jiang J.** Controlling the Nature of Mixed (Phthalocyaninato)(porphyrinato) Rare-Earth(III) Double-Decker Complexes: The Effects of Non-peripheral Alkoxy Substitution of the Phthalocyanine Ligand. *Chem. Eur. J.* 2006. V. 12. P. 1475–1485.
24. **Jiang J., Kasuga K., Arnold D.P.** Sandwich-type Phthalocyaninato and Porphyrinato Metal Complexes. In: Supramolecular Photosensitive and Electroactive Materials. Ed. by H.S. Nalwa. New York: Academic Press. 2001. Chap. 2. P. 113–210.
25. **Asano Y., Muranaka A., Fukasawa A., Hatano T., Uchiyama M., Kobayashi N.** anti-[2.2](1,4)Phthalocyaninophane: Spectroscopic Evidence for Transannular Interaction in the Excited States. *J. Am. Chem. Soc.* 2007. V. 129. P. 4516-4517.
26. (a) **Scholes G.D., Fleming G.R.** On the Mechanism of Light Harvesting in Photosynthetic Purple Bacteria: B800 to B850 Energy Transfer. *J. Phys. Chem. B.* 2000. V. 104. P. 1854-1868. (b) **Jordanides X.J., Scholes G.D., Fleming G.R.** The Mechanism of Energy Transfer in the Bacterial Photosynthetic Reaction Center. *J. Phys. Chem. B.* 2001. P. 105. P. 1652-1669.
27. **Kobayashi N.** Dimers, Trimers, and Oligomers of Phthalocyanines and Related Compounds. *Coord. Chem. Rev.* 2002. V. 227. P. 129-152.
28. **Kobayashi N.** Synthesis and Spectroscopic Properties of Phthalocyanine Analogues. In: Handbook of Porphyrins and Related Macrocycles. Ed. by K.M. Kadish, K.M. Smith, R. Guilard. New York: Academic Press. 2002. V. 15. Chap. 100. P. 161-262.
29. **Kameyama K., Morisue M., Satake A., Kobuke Y.** Highly Fluorescent Self-Coordinated Phthalocyanine Dimers. *Angew. Chem., Int. Ed.* 2005. V. 44. P. 4763-4766.
30. **Kobayashi N., Fukuda T., Lelievre D.** Band Deconvolution Analysis of the Absorption and Magnetic Circular Dichroism Spectral Data of a Planar Phthalocyanine Dimer. *Inorg. Chem.* 2000. V. 39. P. 3632-3637.
31. Modern Cyclophane Chemistry. Ed. by R. Gleiter, H. Hopf. Weinheim, Germany: VCH. 2004.
32. **Kasha M., Rawls H.R., El-Bayoumi M.A.** The Exciton Model in Molecular Spectroscopy. *Pure Appl. Chem*. 1965. V. 11. P. 371-392.
33. **Liu Q., Shimizu S., Kobayashi N.** Cyclophanes Containing Bowl-Shaped Aromatic Chromophores: Three Isomers of *anti*-[2.2](1,4)Subphthalocyaninophane. *Angew. Chem. Int. Ed.* 2015. V. 54. P. 5187-5191.
34. **Hope H., Trueblоо K.N., Bernstein J.** The Crystal and Molecular Structure of 1,1,2,2,9,9,10,10-Octafluoro-[2,2]Paracyclophane and a Reinvestigation of the Structure of [2,2]Paracyclophane. *Crystallogr. Sect. B.* 1972. V. 28. P. 1733-1743.
35. **Kaito A., Nozawa T., Yamamoto T., Hatano M., Orii Y.** LCAO MO SCF π-Electron Calculations on the Magnetic Circular Dichroism of Porphyrin, Protoporphyrin, and Porphyrin a. *Chem. Phys. Lett.* 1977. V. 52. P. 154-160.
36. Although the transition energies were slightly overestimated, use of the long-range corrected CAM-B3LYP exchange-correlation functional for the TDDFT calculations reproduced well the splitting of the Q band on going from CC to CV and further to VV: **Yanai T., Tew D.P., Handy N.C.** A New Hybrid Exchange–Correlation Functional Using the Coulomb-Attenuating Method (CAM-B3LYP). *Chem. Phys. Lett.* 2004. V. 393. P. 51-57.
37. **Kobayashi N., Lam H., Nevin W.A., Janda P., Leznoff C.C., Koyama T., Monden A., Shirai H.** Synthesis, Spectroscopy, Electrochemistry, Spectroelectrochemistry, Langmuir-Blodgett Film Formation, and Molecular Orbital Calculations of Planar Binuclear Phthalocyanines. *J. Am. Chem. Soc.* 1994. V. 116. P. 879-890.
38. **Shibata N., Mori S., Hayashi M., Ueda M., Tokunaga E., Shiro M., Sato H., Hoshi T., Kobayashi N.** A Phthalocyanine-Subphthalocyanine Heterodinuclear Dimer: Comparison of Spectroscopic Properties with Those of Homodinuclear Dimers of the Constituting Units. *Chem. Commun.* 2014. V. 50. P. 3040-3043.
39. **Mack J., Liang X., Dubinina T.V., Tomilova J.G., Nyokong T., Kobayashi N.** MCD Spectroscopy and TD-DFT Calculations of a Naphthalene-ring-bridged Coplanar Binuclear Phthalocyanine Dimer. *J. Porph. Phthal.* 2013. V. 17. P. 489-500.
40. **Asano Y., Sato J., Furuyama T., Kobayashi N.** A Zinc Gable Phthalocyanine and a Derived Planar Bis-Phthalocyanine Containing a Shared Anthracene Unit. *Chem. Commun.* 2012. V. 48. P. 4365-4367.
41. **Leznoff C.C., Lam H., Marcuccio S.M., Nevin W.A., Janda P., Kobayashi N., Lever A.B.P.** A Planar Binuclear Phthalocyanine and Its Dicobalt Derivatives. *Chem. Soc., Chem. Commun*. 1987. P. 699-701.
42. All calculations were performed at the DFT level or ZINDO/S Hamiltonian, implemented in Gaussian 09. The model structures (*tert*-butyl groups were omitted, 1', 2', and 3') were used as model structures. **Frisch M.J., Trucks G.W., Schlegel H.B., Scuseria G.E., Robb M.A., Cheeseman J.R., Scalmani G., Barone V., Mennucci B., Petersson G.A., Nakatsuji H., Caricato M., Li X., Hratchian H.P., Izmaylov A.F., Bloino J., Zheng G., Sonnenberg J.L., Hada M., Ehara M., Toyota K., Fukuda R., Hasegawa J., Ishida M., Nakajima T., Honda Y., Kitao O., Nakai H., Vreven T., Montgomery J.A., Jr., Peralta J.E., Ogliaro F., Bearpark M., Heyd J.J., Brothers E., Kudin K.N., Staroverov V.N., Kobayashi R., Normand J., Raghavachari K., Rendell A., Burant J.C., Iyengar S.S., Tomasi J., Cossi M., Rega N., Millam J.M., Klene M., Knox J.E., Cross J.B., Bakken V., Adamo C., Jaramillo J., Gomperts R., Stratmann R.E., Yazyev O., Austin A.J., Cammi R., Pomelli C., Ochterski J.W., Martin R.L., Morokuma K., Zakrzewski V.G., Voth G.A., Salvador P., Dannenberg J.J., Dapprich S., Daniels A.D., Farkas Ö., Foresman J.B., Ortiz J.V., Cioslowski J., Fox D.J.** Gaussian 09, Revision E.01. Gaussian, Inc. Wallingford CT. 2009.
43. **Ito S., Nakamoto K., Uno H., Murashima T., Ono N.** Synthesis of a Gable Bis-Porphyrin Linked with a Bicyclo[2.2.2]octadiene Ring and Its Conversion into a Conjugated Planar Bis-Porphyrin. *Chem. Commun.* 2001. P. 2696-2697.
44. **Ishii K., Abiko S., Fujitsuka M., Ito O., Kobayashi N.** Exciton Interactions in a Self-Assembled Phthalocycnine Dimer. *J. Chem. Soc., Dalton Trans.* 2002. P. 1735-1739.
45. **Muranaka A., Asano Y., Tsuda A., Osuka A., Kobayashi N.** Spectroscopic and Theoretical Studies of Optically Active Porphyrin Dimers: A System Uninterpretable by Exciton Coupling Theory. *Chem. Phys. Chem.* 2006. V. 7. P. 1235-1240.
46. **Kobayashi N., Muranaka A., Mack J.** Circular Dichroism and Magnetic Circular Dichroism for Organic Chemists (textbook). London: Royal Society of Chemistry. 2012 (comments in Angew. Chem. Int. Ed. 2012. V. 51. P. 10446).
47. **Harada N., Ono H., Uda H., Parveen M., Khan N.U-P., Achari B.P.K.** Atropisomerism in Natural Products. Absolute

stereochemistry of Biflavone, (-)-4',4''',7,7''-Tetra-O-Methylcupressuflavone, as Determined by the Theoretical Calculation of CD Spectra. *J. Am. Chem. Soc.* 1992. V. 114. P. 7687–7692.

48. **Furche F., Ahlrichs R., Wachsmann C., Weber E., Sobanski A., Vçgtle F., Grimme S.** Circular Dichroism of Helicenes Investigated by Time-Dependent Density Functional Theory. *J. Am. Chem. Soc.* 2000. V. 122. P. 1717-1724.
49. **Diedrich C., Grimme S.** Systematic Investigation of Modern Quantum Chemical Methods to Predict Electronic Circular Dichroism Spectra. *J. Phys. Chem. A.* 2003. V. 107. P. 2524-2539.
50. **Toyota S., Shimasaki T., Tanifuji N., Wakamatsu K.** Experimental and Theoretical Investigations of Absolute Stereochemistry and Chiroptical Properties of Enantiopure 2,2'-Substituted 9,9'-Bianthryls. *Tetrahedron: Asymmetry*. 2003. V. 14. P. 1623-1629.
51. **Tsuda A., Furuta H., Osuka A.** Syntheses, Structural Characterizations, and Optical and Electrochemical Properties of Directly Fused Diporphyrins. *J. Am. Chem. Soc.* 2001. V. 123. P. 10304-10321.
52. **Muranaka A., Yokoyama M., Matsumoto Y., Uchiyama M., Tsuda A., Osuka A., Kobayashi N.** Magnetic Circular Dichroism Study of Directly Fused Porphyrins. *Chem. Phys. Chem.* 2005. V. 6. P. 171-179.
53. **Fukuda T., Biyajima T., Kobayashi N.** A Discrete Quadruple-Decker Phthalocyanine. *J. Am. Chem. Soc.* 2010. V. 132. P. 6278-6279.
54. (a) **Weiss R., Fischer J.** Lanthanide Phthalocyanine Complexes. In: The Porphyrin Handbook. Ed. by K.M. Kadish, K.M. Smith, R. Guilard. San Diego: Academic Press. 2003. V. 16. Chap. 105. pp 171-246. (b) **Buchler J.W., Ng D.K.P.** Metal Tetrapyrrole Double- and Triple-Deckers with Special Emphasis on Porphyrin Systems. In: The Porphyrin Handbook. Ed. by K.M. Kadish, K.M. Smith, R. Guilard. San Diego: Academic Press. 2003. V. 3. Chap. 20. P. 245-294.
55. **George R.D., Snow A.W., McMillan P.F., Burrows V.A.** Synthesis and Characterization of an Oligomeric Mercury-Bridged Phthalocyanine. *J. Am. Chem. Soc.* 1992. V. 114. P. 8286-8287.
56. **Chambrier I., White G.F., Cook M.J.** Oligomeric Cadmium–Phthalocyanine Complexes: Novel Supramolecular Free Radical Structures. *Chem. Eur. J.* 2007. V. 13. P. 7608-7618.
57. **Kobayashi N.** Spectroscopically and/or Structurally Intriguing Phthalocyanines and Related Compounds. Part 1. Monomeric systems. *Izv. Vyssh. Uchebn. Zaved. Khim. Khim. Tekhnol.* [*Russ. J. Chem. & Chem. Tech.*]. 2019. V. 62. N 4. P. 4-46.
58. **Konami H., Hatano M., Tajiri A.** An Analysis of Paramagnetic Shifts in Proton MNR Spectra of Non-Radical Lanthanide(III)-Phthalocyanine Sandwich Complexes. *Chem. Phys. Lett.* 1989. V. 160. P.163-167.
59. **Ishikawa N.** Electronic Structures and Spectral Properties of Double- and Triple- Decker Phthalocyanine Complexes in a Localized Molecular Orbital View. *J. Porph. Phthal.* 2001. V. 5. P. 87-101.
60. (a) **Guyon F., Pondaven A., Kerbaol J.M., L'Her M.** From the Single- to the Triple-Decker Sandwich. Effect of Stacking on the Redox and UV−Visible Spectroscopic Properties of Lutetium(III) 1,2-Naphthalocyaninate Complexes. *Inorg. Chem.* 1998. V. 37. P. 569-576. (b) **Dewulf D.W., Leland J.K., Wheeler B.L., Bard A.J., Batzel D.A., Dininny D.R., Kenney M.E.** Spectral Study of Tris(β-dionato)cobalt(III) Chelates. Structure-Redox Potential Relations. *Inorg. Chem.* 1987. V. 26. P. 26-32.
61. **Nakamura Y., Aratani N., Shinikubo H., Takagi A., Kawai T., Matsumoto T., Kim D., Muranaka A., Kobayashi N., Osuka A.** A Directly Fused Tetrameric Porphyrin Sheet and Its Anomalous Electronic Properties That Arise from the Planar Cyclooctatetraene Core. *J. Am. Chem. Soc.* 2006. V. 128. P. 4119-4127.
62. **Nakamura Y., Hwang I.-W., Aratani N., Ahn T.K., Ko D.M., Takagi A., Kawai T., Matsumoto T., Kim D., Osuka A.** Directly meso−meso Linked Porphyrin Rings: Synthesis, Characterization, and Efficient Excitation Energy Hopping. *J. Am. Chem. Soc.* 2005. V. 127. P. 236-246.
63. **Kobayashi N**. Spectroscopically and/or Structurally Intriguing Phthalocyanines and Related Compounds. Part 2. Monomeric Systems. *Izv. Vyssh. Uchebn. Zaved. Khim. Khim. Tekhnol.* [*Russ. J. Chem. & Chem. Tech.*]. 2019. V. 62. N 8. P. 4-25.

Поступила в редакцию 17.09.2019
Принята к опубликованию 07.10.2019

Received 17.09.2019
Accepted 07.10.2019